AUTHOR QUERY FORM

Journal: CELL

Article Number: 9573

Dear Author,

Please check your proof carefully and mark all corrections at the appropriate place in the proof.

Location in article	Query / Remark: Click on the Q link to find the query's location in text Please insert your reply or correction at the corresponding line in the proof
Q1	Could you please provide the grant number for (1) Public Health Agency of Canada and (2) DAAD, if any?

Thank you for your assistance.

Article

Cell

Antibodies from a Human Survivor Define Sites of Vulnerability for Broad Protection against Ebolaviruses

Graphical Abstract

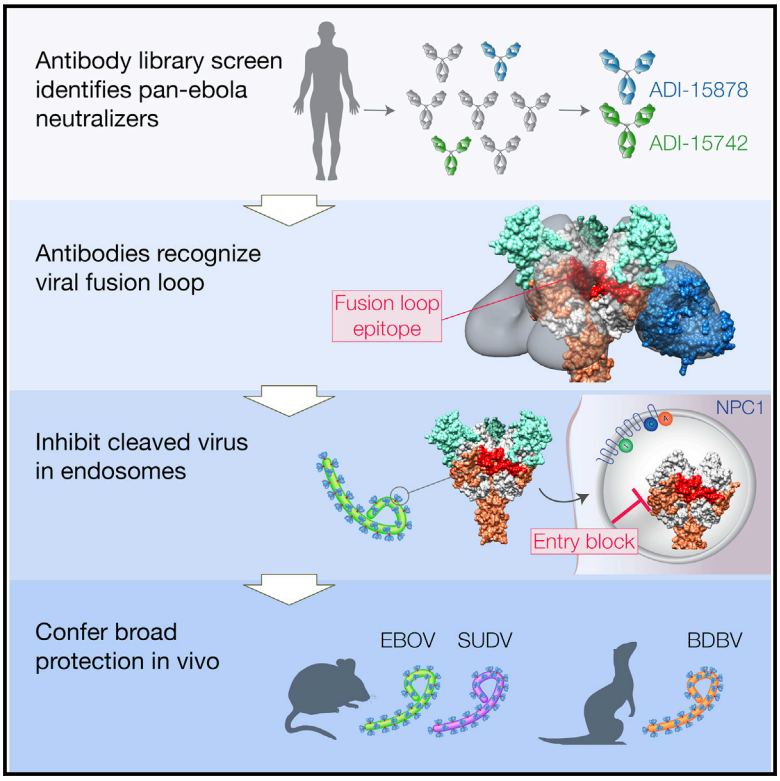

Highlights

- The human humoral response to Ebola virus contains broadly neutralizing antibodies
- Potent pan-Ebola neutralizing antibodies recognize the viral fusion loop
- The antibodies target viral entry intermediate generated in endosomes
- The antibodies protect against ~~Ebola virus species~~ that cause outbreaks in humans

Authors

Anna Z. Wec, Andrew S. Herbert, Charles D. Murin, ..., John M. Dye, Kartik Chandran, Zachary A. Bornholdt

Correspondence

john.m.dye1.civ@mail.mil (J.M.D.), kartik.chandran@einstein.yu.edu (K.C.), zachary.bornholdt@mappbio.com (Z.A.B.)

In Brief

Characterization of human pan-reactive neutralizing antibodies against all five species of Ebola virus highlights the fusion loop region of the viral glycoprotein as a promising vaccine target.

Wec et al., 2017, Cell *169*, 1–13
May 18, 2017
http://dx.doi.org/10.1016/j.cell.2017.04.037

CellPress

Please cite this article in press as: Wec et al., Antibodies from a Human Survivor Define Sites of Vulnerability for Broad Protection against Ebolaviruses, Cell (2017), http://dx.doi.org/10.1016/j.cell.2017.04.037

Cell

Antibodies from a Human Survivor Define Sites of Vulnerability for Broad Protection against Ebolaviruses

Anna Z. Wec,[1,10] Andrew S. Herbert,[2,10] Charles D. Murin,[3,4] Elisabeth K. Nyakatura,[5] Dafna M. Abelson,[6] J. Maximilian Fels,[1] Shihua He,[7,8] Rebekah M. James,[2] Marc-Antoine de La Vega,[7,8] Wenjun Zhu,[7,8] Russell R. Bakken,[2] Eileen Goodwin,[9] Hannah L. Turner,[3] Rohit K. Jangra,[1] Larry Zeitlin,[6] Xiangguo Qiu,[7,8] Jonathan R. Lai,[5] Laura M. Walker,[9] Andrew B. Ward,[3] John M. Dye,[2,11,*] Kartik Chandran,[1,11,12,*] and Zachary A. Bornholdt[6,11,13,*]

[1]Department of Microbiology and Immunology, Albert Einstein College of Medicine, Bronx, NY 10461, USA
[2]U.S. Army Medical Research Institute of Infectious Diseases, Fort Detrick, MD 21702, USA
[3]Department of Integrative Structural and Computational Biology, The Scripps Research Institute, La Jolla, CA 92037, USA
[4]Department of Immunology and Microbial Science, The Scripps Research Institute, La Jolla, CA 92037, USA
[5]Department of Biochemistry, Albert Einstein College of Medicine, Bronx, NY 10461, USA
[6]Mapp Biopharmaceutical, San Diego, CA 92121, USA
[7]Special Pathogens Program, National Microbiology Laboratory, Public Health Agency of Canada, Winnipeg, MB R3E 3R2, Canada
[8]Department of Medical Microbiology, University of Manitoba, Winnipeg, MB R3E 0J9, Canada
[9]Adimab, LLC, Lebanon, NH 03766, USA
[10]These authors contributed equally
[11]Senior Author
[12]Twitter: @chandranlab
[13]Lead Contact
*Correspondence: john.m.dye1.civ@mail.mil (J.M.D.), kartik.chandran@einstein.yu.edu (K.C.), zachary.bornholdt@mappbio.com (Z.A.B.)
http://dx.doi.org/10.1016/j.cell.2017.04.037

SUMMARY

Experimental monoclonal antibody (mAb) therapies have shown promise for treatment of lethal Ebola virus (EBOV) infections, but their species-specific recognition of the viral glycoprotein (GP) has limited their use against other divergent ebolaviruses associated with human disease. Here, we mined the human immune response to natural EBOV infection and identified mAbs with exceptionally potent pan-ebolavirus neutralizing activity and protective efficacy against three virulent ebolaviruses. These mAbs recognize an inter-protomer epitope in the GP fusion loop, a critical and conserved element of the viral membrane fusion machinery, and neutralize viral entry by targeting a proteolytically primed, fusion-competent GP intermediate (GP_{CL}) generated in host cell endosomes. Only a few somatic hypermutations are required for broad antiviral activity, and germline-approximating variants display enhanced GP_{CL} recognition, suggesting that such antibodies could be elicited more efficiently with suitably optimized GP immunogens. Our findings inform the development of both broadly effective immunotherapeutics and vaccines against filoviruses.

INTRODUCTION

Viruses of the family *Filoviridae* (filoviruses) cause outbreaks of a lethal disease for which no Food and Drug Administration (FDA)-approved treatments or vaccines are available. The unprecedented 2013–2016 Ebola virus (EBOV) epidemic in Western Africa highlighted the potential of these agents to cause health emergencies of international scope and has accelerated the development of countermeasures (de La Vega et al., 2015; Kuhn et al., 2014). At the height of this epidemic, several early-stage therapeutics and vaccines were evaluated under compassionate-use protocols (Wong and Kobinger, 2015). Arguably the most successful of these is ZMapp, an immunotherapeutic comprising three mouse/human chimeric monoclonal antibodies (mAbs), c2G4, c4G7, and c13C6, which target the glycoprotein (GP) spikes on the surface of EBOV virions. ZMapp was highly effective at reversing advanced EBOV disease (EVD) in non-human primates (NHPs) and provided initial evidence of efficacy in a phase II clinical trial (Davey et al., 2016; Qiu et al., 2014). Despite its promise, ZMapp suffers a key limitation. It lacks activity against other filoviruses associated with human disease, including Bundibugyo virus (BDBV), Sudan virus (SUDV), and Marburg virus (MARV), because its component mAbs do not recognize and neutralize these divergent GPs (Murin et al., 2014). The public health threat represented by BDBV and SUDV, which caused ≈40% of all ebolavirus infections prior to 2013 (Burk et al., 2016), and by newly emerging or engineered ebolaviruses, demands an urgent response.

Given the scientific and logistical hurdles inherent in developing a separate mAb therapeutic for each filovirus, recent work has focused on the development of broadly protective immunotherapies. Frei et al. (2016) combined known EBOV and SUDV GP-specific neutralizing antibodies (NAbs) KZ52 and a humanized variant of 16F6 ~~and F4~~, respectively, to generate bispecific antibodies that protected against both viruses in mice. More recently, bispecific antibodies combining two broadly reactive

but non-neutralizing mAbs targeting virus:host receptor interactions were shown to neutralize all known ebolaviruses through a "Trojan horse" mechanism and to protect mice challenged with EBOV or SUDV (Wec et al., 2016). The presence of cross-reactive and cross-neutralizing antibodies in natural antibody repertoires following monospecific ebolavirus infection or immunization has also been noted (Bornholdt et al., 2016b; Macneil et al., 2011; Natesan et al., 2016), and antibody discovery efforts have yielded cross-neutralizing mAbs with increased protective breadth (Flyak et al., 2016; Furuyama et al., 2016; Howell et al., 2016; Keck et al., 2015). To date, however, only a single canonical IgG with true pan-ebolavirus neutralizing activity—the mouse mAb 6D6—has been reported (Furuyama et al., 2016). Moreover, no natural or engineered antibody has yet been shown to protect animals against EBOV, BDBV, and SUDV (Burk et al., 2016).

Here, we sought to perform a systematic analysis of the breadth of the anti-ebolavirus neutralizing mAb response in humans. Accordingly, we screened our recently published library of 349 human mAbs isolated from a survivor of the recent West African EBOV outbreak (Bornholdt et al., 2016b) for broad neutralizers. We identified two mAbs that could potently neutralize all five ebolaviruses and confer post-exposure protection against EBOV, BDBV, and SUDV in animal challenge models. Follow-up studies indicated that these mAbs recognize a hitherto unknown GP epitope that encompasses membrane-seeking residues in the internal fusion loop and mediate neutralization by targeting a proteolytically cleaved GP intermediate in the endocytic pathway. Together, our findings inform the development of pan-ebolavirus immunotherapeutics and the design of filovirus vaccines tailored to elicit highly potent cross-protective antibodies.

RESULTS

Identification of Cross-Reactive and Cross-Neutralizing mAbs

To identify broadly reactive mAbs in the EVD survivor library, we screened recombinant VSV (rVSV) particles displaying prototypic GPs from EBOV, BDBV, and SUDV by ELISA. 72% of the mAbs recognized BDBV GP, whereas only 11% cross-reacted with SUDV GP (Figure S1A), consistent with the amino acid sequence conservation among these GPs. 37 of 349 mAbs reacted with all three GPs by ELISA (Figure S1B). Within this subset, 16 mAbs belonged to the glycan cap epitope group (c13C6 competitors), 10 mAbs targeted the GP base (KZ52 competitors), another 10 were directed against the α-helical heptad repeat 2 in the GP2 "stalk" (HR2 epitope group, ADI-15974 competitors), and one mAb belonged to an undefined but GP1-specific epitope group (Bornholdt et al., 2016b).

We assayed the 37 cross-reactive mAbs for their capacity to inhibit infection by rVSV particles bearing SUDV GP, the most divergent from EBOV GP in amino acid sequence. Neutralization potency was first evaluated at two concentrations, and mAbs advanced if >50% reduction in infection was observed at the higher dose (Figures S1C–S1F). Only 10 of 37 cross-reactive mAbs showed significant neutralizing activity against rVSV-SUDV GP. Six of these NAbs belonged to the KZ52 competition group and targeted the GP base, whereas the remaining four were equally divided between the HR2 and 13C6 epitope groups (Figures 1A and S1C–S1F). These and previous results (Flyak et al., 2016) suggest that a small subset of cross-reactive and cross-neutralizing antibodies is generated by the human immune response in the course of natural ebolavirus infection.

Analysis of mAb Neutralization Breadth In Vitro

To evaluate the breadth and potency of neutralization by the top ten NAbs identified above, we performed dose-response neutralization assays with rVSVs bearing GPs from all five known ebolaviruses—EBOV, BDBV, SUDV, Reston virus (RESTV), and Taï Forest virus (TAFV) (Figures 1B–1P; Table S1). The HR2 binder, ADI-16061, potently neutralized infection by rVSVs bearing EBOV, BDBV, and TAFV GP with half-maximal inhibitory concentration (IC_{50}) values below 5 nM but had little activity against those bearing SUDV and RESTV GP. The second NAb from this group, ADI-15975, possessed an even narrower antiviral spectrum, with strong activity only against rVSV-EBOV GP (Figures 1B, 1E, 1H, 1K, and 1N; Table S1).

The glycan cap binders, ADI-15750 and ADI-15968, neutralized rVSVs bearing EBOV, TAFV, and SUDV GP, albeit with weaker activity against SUDV GP (Figures 1C, 1I, 1L; Table S1). Further, ADI-15750 was effective at neutralizing rVSV-RESTV GP but not rVSV-BDBV GP, whereas the converse was true for ADI-15968 (Figures 1F and 1O; Table S1). Thus, none of the mAbs directed against the GP stalk or glycan cap demonstrated pan-ebolavirus neutralizing profiles, consistent with the limited antigenic conservation across these GP surfaces (Figures 4, S3A, and S3B).

Two NAbs recognizing the GP base, ADI-15878 and ADI-15742, possessed exceptionally broad and potent neutralizing activity (IC_{50} <2 nM) against all five rVSV-GPs (Figures 1D, 1G, 1J, 1M, and1P; Table S1). A third base-binding NAb, ADI-15946, potently neutralized EBOV, BDBV, and TAFV, but showed reduced or no activity toward rVSVs bearing SUDV and RESTV GP, respectively (Figures 1D, 1G, 1J, 1M, and 1P; Table S1). The remaining three NAbs in this epitope class were not pursued further due to their limited neutralization breadth.

We advanced the broadest and most potent neutralizers in each epitope group for testing against authentic ebolaviruses (Figure 2). The results largely corroborated our findings with rVSV-GPs and confirmed that only the base binders ADI-15878 and ADI-15742 could potently neutralize infection by EBOV, BDBV, and SUDV (IC_{50} ≤1 nM) (Figure 2). However, the activity of these broadly neutralizing Abs (bNAbs) did not extend to the more divergent GPs of Lloviu virus (LLOV) and MARV (Table S1). These findings underscore the challenges inherent in achieving pan-filovirus or even pan-ebolavirus neutralization with single mAbs targeting surface-exposed GP epitopes.

Mapping of bNAb Epitopes Using Negative-Stain Electron Microscopy and Escape Mutant Analysis

To visualize each GP:bNAb complex, we performed negative-stain transmission electron microscopy (EM) studies of the antigen binding fragments (Fabs) of ADI-16061, ADI-15750,

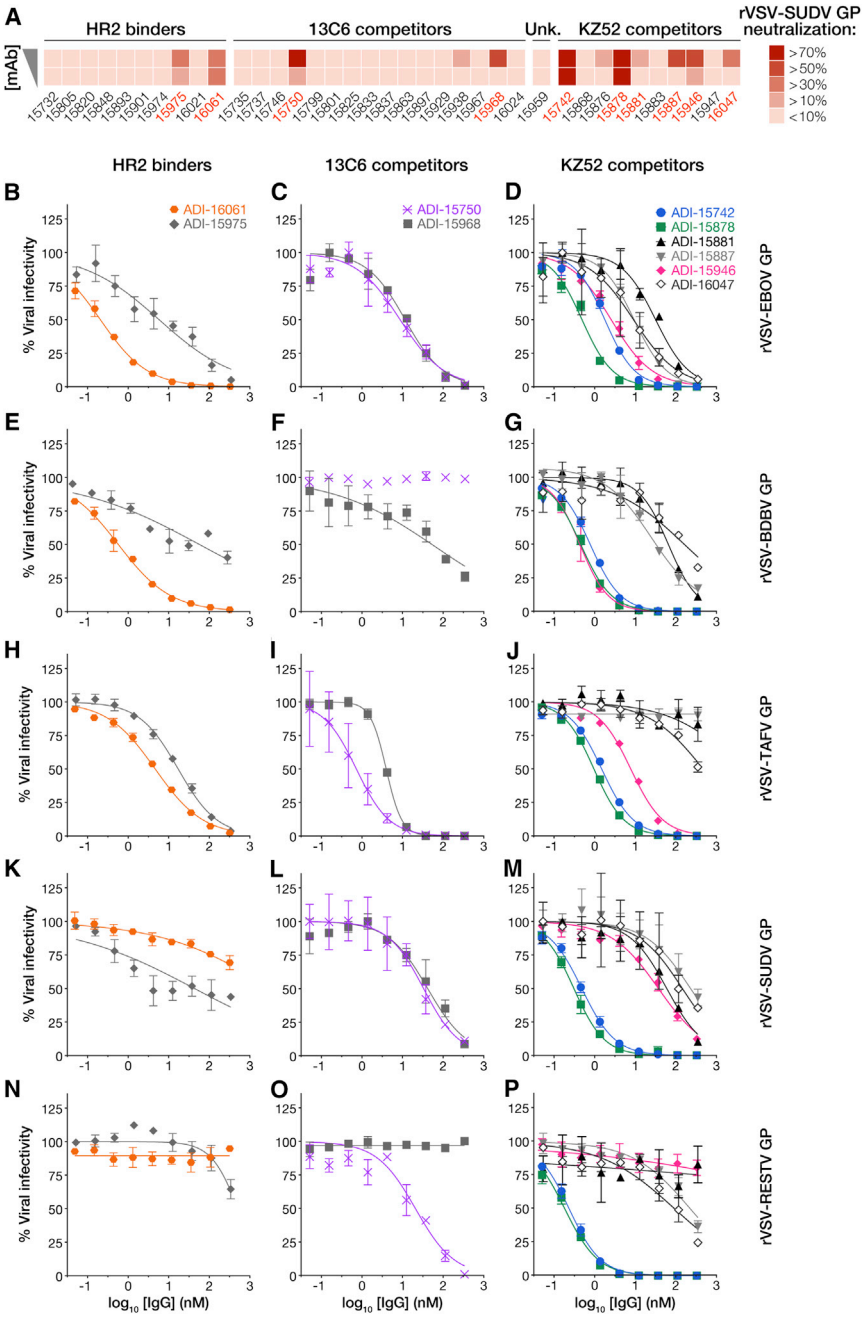

Figure 1. Identification of bNAbs from a Human Survivor of EBOV Infection

(A) Heatmap of rVSV-SUDV GP neutralization activity by cross-reactive mAbs from a human EVD survivor mAb library. Activity at 330 nM (top) and 33 nM (bottom) of mAb is shown. mAbs with activity at both concentrations are highlighted in red. See also Figure S1.

(B–P) Neutralization of rVSV-GPs by mAbs with SUDV GP-specific neutralizing activity in (A). Means ± SD for three replicates are shown. See also Table S1.

ADI-15878, ADI-15742, and ADI-15946 bound to trimeric soluble EBOV GP (GPΔTM). 3D reconstructions determined from the EM class averages confirmed previous epitope group assignments based on binding competition experiments (Bornholdt et al., 2016b). To approximate bNAb footprints on GP, we fit the recently solved unliganded EBOV GPΔTM X-ray crystal structure (PDB: 5JQ3) (Zhao et al., 2016) into the GP envelope obtained by image reconstruction (Figure 3). Further, to identify GP residues critical for bNAb binding and viral neutralization, we selected neutralization escape mutants (Figures 3, S2, and S3). rVSV-GPs were serially passaged in the presence of each bNAb until complete viral resistance was observed, and the *GP* genes of viral clones were sequenced to identify escape mutations (Figures 3, S2, and S3).

ADI-16061 bound to HR2 and an N-terminal portion of the membrane proximal external region (MPER) between residues 621–640 in the GP2 stalk, with an angle of approach perpendicular to the GP stalk and parallel to the viral membrane (Figure 3A). Despite the compact nature of the GP stalk, three Fabs could bind per GP trimer, each rotated by ~50° with respect to the GP 3-fold symmetry axis. Two independent mutations in HR2, H628N and D632E (Figure 3E), greatly reduced GP:bNAb binding (Figure S2A) and afforded escape from viral neutralization (Figure S2B). While residue H628 was visualized in the EBOV GP X-ray crystal structure (Zhao et al., 2016), the complete ADI-16061 epitope likely extends past the last resolved amino acid residue (631), inclusive of D632E, and into the MPER (EBOV GP residues ≈633–657). The high degree of viral species-dependent sequence variation in the MPER probably accounts for the failure of ADI-16061 to neutralize RESTV and SUDV (Figures 1, 2, and S3A).

Complexes between ADI-15750 and GPΔTM were not amenable to 3D reconstruction due to partial mAb occupancy, likely resulting from poor binding affinity (data not shown). However, 2D class averages of these complexes showed the Fabs binding GP axially to the viral membrane, reminiscent of the binding modes of c13C6 and other glycan cap binders (Bornholdt et al., 2016b; Murin et al., 2014; Pallesen et al., 2016) (Figure S4A). rVSV-EBOV GP particles escaped ADI-15750 neutralization via mutation of multiple glycan cap residues that compromised GP:bNAb binding to varying degrees (Figures S2, S3, and S4). The ADI-15750 binding footprint inferred from the escape mutant analysis appears to overlap that of mAb c13C6 (Pallesen et al., 2016) (Figures 4D, 4E, S3, and S4).

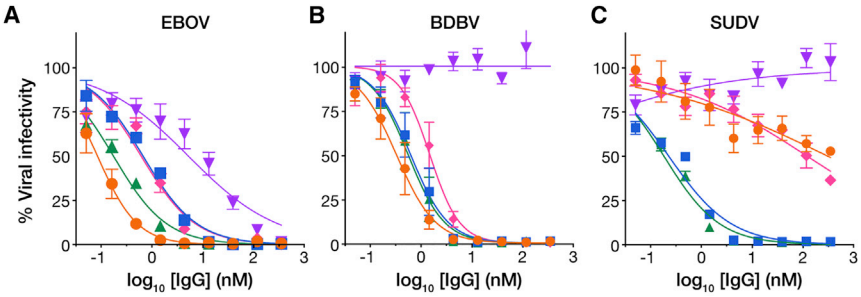

Figure 2. Potency and Breadth of Authentic Ebolavirus Neutralization by Human bNAbs

(A–C) Neutralization of authentic EBOV (A), BDBV (B), and SUDV (C) by lead bNAbs identified in Figure 1. Means ± SD for three replicates are shown.

(D) Summary of authentic ebolavirus neutralization. IC_{50}, mAb concentration that affords half-maximal neutralization of viral infectivity. Hyphens indicate no detectable neutralizing activity.

D

Authentic virus neutralization IC_{50} (nM)			
mAb	EBOV	BDBV	SUDV
HR2/Stalk Binding Group			
ADI-16061	0.1	0.3	300
13C6 Competition Group (glycan cap binders)			
ADI-15750	5.2	–	–
KZ52 Competition Group (base binders)			
ADI-15742	0.7	0.6	0.2
ADI-15878	0.2	0.6	0.2
ADI-15946	0.6	1.5	120

ADI-16061 | HR2 binder
ADI-15750 | 13C6 competitor
ADI-15742, ADI-15878, ADI-15946 | KZ52 competitors

Concordantly, binding of both mAbs was sensitive to the G271R escape mutation engendered by ADI-15750 (Figures S4C and S4D).

The GP base-binding bNAbs ADI-15878 and ADI-15742 are clonal siblings with 90% and 95% identity in their variable heavy (V_H) and variable light (V_L) amino acid sequences, respectively (Bornholdt et al., 2016b) (Figure 6A). Their Fabs showed a steep angle of approach similar to the SUDV-monospecific Fab 16F6 (Dias et al., 2011) but appeared to be rotated by ≈90° about their long axes relative to the EBOV-monospecific Fab KZ52 (Figures 3B, 3C, and 3I) (Lee et al., 2008b). The epitope targeted by ADI-15878 and ADI-15742 is also rotated by ≈60° about the GP 3-fold symmetry axis relative to the base binders KZ52, 16F6, c2G4, and c4G7 (Dias et al., 2011; Lee et al., 2008a; Murin et al., 2014; Pallesen et al., 2016) (Figures 3B, 3C, 3I, and 4). The ADI-15878/15742 footprint on GP comprises discontinuous sequences in both GP1 and GP2 subunits that span neighboring protomers, including putative membrane-seeking residues in the highly conserved GP2 internal fusion loop (IFL) (Figures 3B, 3C, and 4). Consistent with a critical role for bNAb:IFL contacts, a single IFL point mutation, G528E, abolished both viral recognition and neutralization without observable effects on viral entry (Figures 3F, 3G, S2, and S3). Both ADI-15742 and ADI-15878, like another base-binding NAb mAb-100, are also predicted to contact the complex N-liked glycan at GP2 residue 563, in the α-helical heptad repeat 1 (HR1) sequence of the adjacent protomer (Figures 3B, 3C, 3F, 3G, and 4B) (Misasi et al., 2016). Glycosylation of this residue is strictly conserved across all filovirus GPs (Figure S3).

Unexpectedly, ADI-15878/15742 displayed enhanced binding and neutralization of rVSV-EBOV GP particles bearing the N563A mutation, indicating that the glycan on this residue impairs GP recognition. By contrast, removal of the N563 glycan abolished mAb-100 neutralization and modestly reduced the activity of the other base binders tested (Figures 5D, S5D, S5E, and S5F).

ADI-15946, the third base-binding bNAb identified herein, targets an epitope that is similarly positioned to those of mAbs KZ52, c2G4, and c4G7 (Lee et al., 2008a; Murin et al., 2014; Pallesen et al., 2016) but shifted upward toward the glycan cap (Figures 3D and 4F–4H). ADI-15946's angle of approach is similar to that of mAb c2G4 (Murin et al., 2014; Pallesen et al., 2016) and its contacts involve discontinuous sequences with a single GP protomer: GP1 base (residues 71–77), glycan cap (residues 251–303), and GP2 (residues 508–514) (Figures 3D and 4F). A single amino acid change (K510E), adjacent to the KZ52/c2G4/c4G7 escape mutation (Q508R) (Audet et al., 2014), afforded complete viral resistance to ADI-15946 binding and neutralization (Figures 3D, 3H, S2, and S3). A second mutation at a buried position in the GP1 base (E100K) weakened viral neutralization but did not substantially diminish ADI-15946:GP binding. The higher level of sequence conservation in the putative ADI-15946 epitope relative to those of c2G4, C4G7, and KZ52 likely explains the former's enhanced antiviral breadth (Figures 4F and S3D). However, the greater sequence divergence of SUDV and RESTV GP at the proposed sites of contact (Figure S3) is consistent with the failure of ADI-15946 to neutralize viruses bearing these GPs.

Mechanisms of Antiviral Neutralization

The filovirus cell entry pathway is a complex, multistep process that culminates in GP-catalyzed fusion between viral and host endosomal membranes and escape of a viral nucleocapsid payload into the cytoplasm (reviewed in Miller and Chandran, 2012; Moller-Tank and Maury, 2015). Following their attachment to the plasma membrane of a permissive cell, virions are internalized and trafficked to late endo/lysosomal compartments (Simmons et al., 2015; Spence et al., 2016). In endosomes, resident host cysteine cathepsins cleave GP to remove the mucin and glycan cap sequences (Chandran et al., 2005; Schornberg et al., 2006), thereby unmasking a binding site for the critical endosomal receptor, Niemann-Pick C1 (NPC1) (Bornholdt et al., 2016a; Carette et al., 2011; Côté et al., 2011; Miller et al., 2012). Recognition of NPC1 by a cleaved GP species (hereafter, GP_{CL}), together with one or more unknown host signals, is proposed to trigger GP refolding and the membrane fusion reaction that is coupled to it (Brecher et al., 2012; Miller et al., 2012; Spence et al., 2016; Wong et al., 2010).

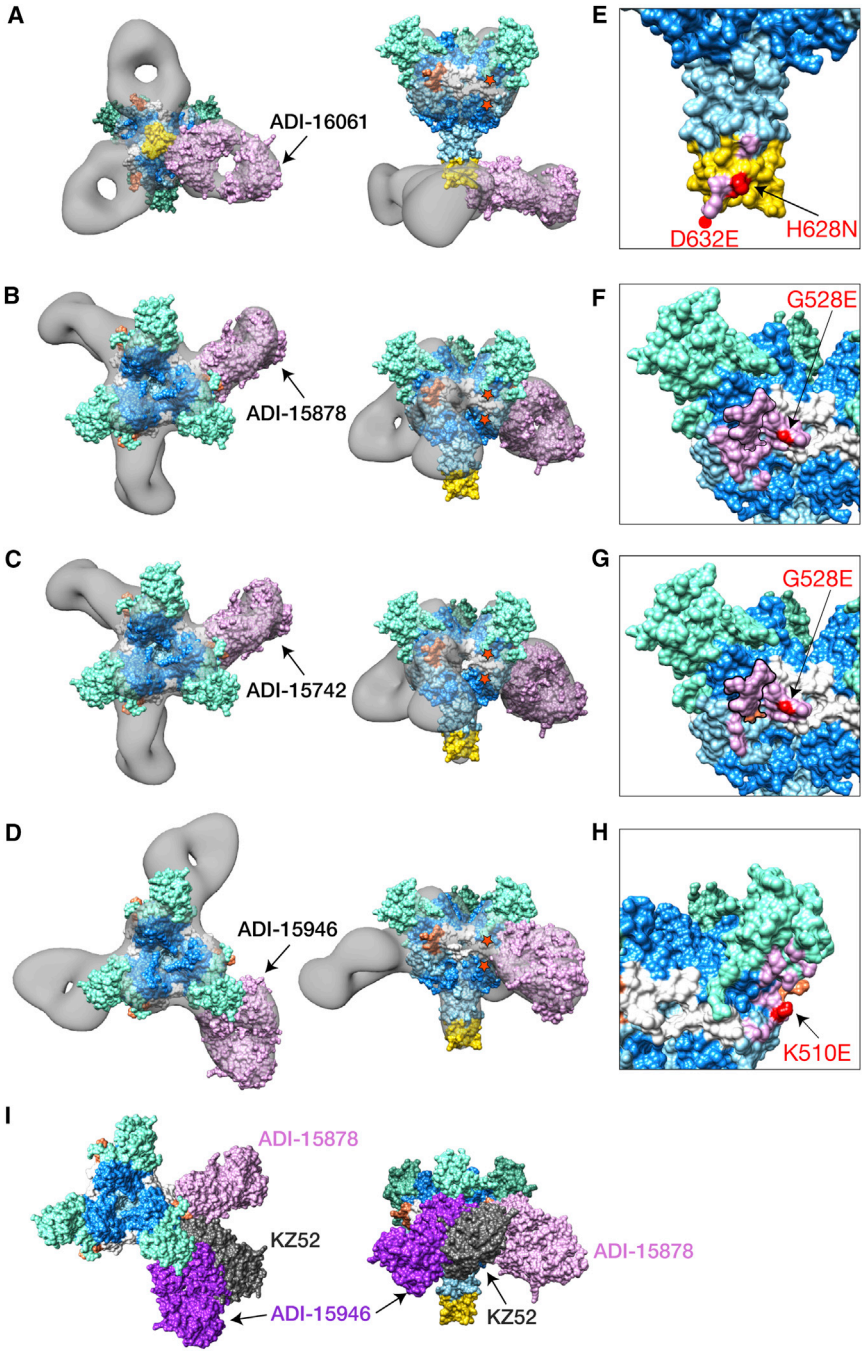

Figure 3. Negative-Stain Electron Microscopy of Fab: EBOV GPΔTM Complexes

(A–D) 3D reconstructions of four Fab:EBOV GPΔTM complexes are shown in transparent surface representation (gray) with a structure-based model of the GPΔTM trimer fitted into the density. Structural subdomains of the GP trimer are labeled as follows: GP1 glycan cap (aqua green), GP1 core (blue), GP2 (light blue), GP2 internal fusion loop region (white), and the stalk/HR2 region (yellow). The conserved glycan on Asn 563 in GP2 is indicated in orange. GP-bound Fabs are shaded in lilac. Top and side views are shown at left and right, respectively, in (A)–(D) and (I). A bottom view of ADI-16061:GP is shown. Orange stars, approximate termini of the β13-β14 loop, connecting the GP1 base and glycan cap.

(E–H) Magnified views of (A)–(D) indicating the putative Fab contact sites on the GPΔTM trimer (lilac). Highlighted residues are located within 5 Å of the Fab model. Black outline, N-linked glycan on Asn 563. Red, residues conferring viral neutralization escape. See also Figures S2 and S3.

(I) 3D reconstructions of ADI-15878 and ADI-15946 are superimposed with a structure-based model of the KZ52 Fab:GPΔTM complex (PDB: 3CSY) (Lee et al., 2008a) to highlight the angle of approach of each base binder.

See also Figure S4.

In initial studies, we found that ADI-15878, ADI-15742, and ADI-15946 were efficiently co-internalized with viral particles and delivered to NPC1$^+$ late endosomes (Figures S5A and S5B for ADI-15878). Because GP_{CL}:NPC1 recognition is an indispensable requirement for filovirus entry (Miller et al., 2012), we first examined the capacity of the GP base-binding bNAbs to inhibit it in a competitive ELISA (Figure 5A). Pre-incubation of each bNAb with VSV particles bearing EBOV GP_{CL} had no effect on viral capture of a soluble fragment of NPC1, whereas the mAbs MR72 and FVM04, which bind directly to the receptor-binding site (RBS) in GP_{CL}, blocked NPC1 capture, as described previously (Bornholdt et al., 2016a; Howell et al., 2016). Thus, consistent with their RBS-distal epitopes, none of the GP base binders described herein exert their antiviral effect by directly preventing the virus-receptor interaction. (Figures 3 and 4).

Endosomal GP → GP_{CL} cleavage is a prerequisite for GP_{CL}:NPC1 binding and therefore essential for filovirus entry. Accordingly, we investigated if any of the NAbs could interfere with this proteolytic processing step, as reported for the human EBOV-specific GP base binders, KZ52 and mAb-100 (Misasi et al., 2016; Shedlock et al., 2010). rVSV-EBOV GP particles were pre-incubated with each NAb and then exposed to the endosomal cysteine protease cathepsin L (CatL). GP cleavage was assessed by measuring exposure of the GP_{CL} RBS with an NPC1-binding ELISA (Figure 5B) or by gel electrophoresis and immunoblotting (Figure 5C) as described (Chandran et al., 2005; Miller et al., 2012). ADI-15946, similar to c2G4, c4G7, KZ52, and mAb-100, could inhibit GP → GP_{CL} cleavage and GP_{CL} RBS exposure in a dose-dependent manner. By contrast, ADI-15878 and ADI-15742 were ineffective at blocking GP → GP_{CL} cleavage. These results are consistent with the proximity of the binding footprints of mAb-100, c2G4, c4G7,

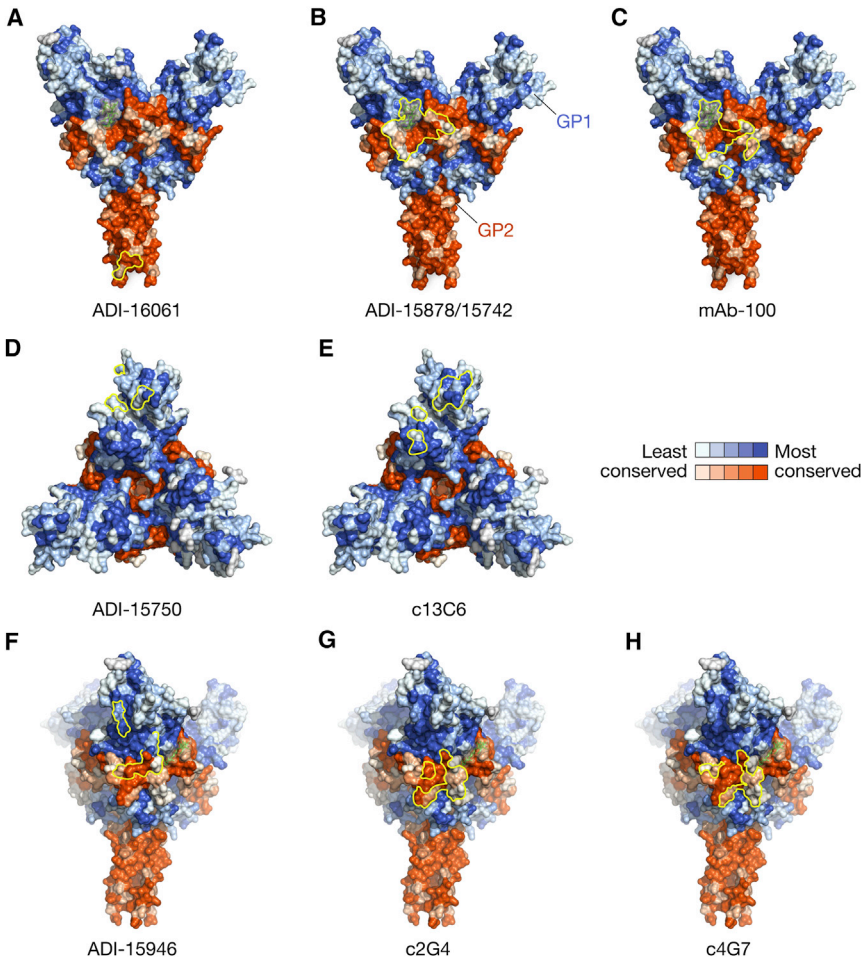

Figure 4. Predicted bNAb Epitopes

The predicted GP:NAb contact surface is indicated as a yellow outline on a surface-shaded representation of the GPΔTM trimer model (PDB: 5JQ3). Each amino acid residue in GP1 (blue) and GP2 (red) is shaded according to the degree of sequence conservation among ebolavirus GP proteins at that position, based on a multiple sequence alignment (light to dark, 0% to 100% sequence identity) (see the STAR Methods for details). In (A)–(C), the N–linked glycan on GP2 residue Asn 563 is indicated as a translucent envelope and green balls-and-sticks. Antibody contact sites in (C), (E), (G), and (H) are derived from published structures of EBOV GP:Fab complexes.

and ADI-15946 to the GP1 β13-β14 loop, which is proposed to be the initial target of proteolytic cleavage (Chandran et al., 2005; Dube et al., 2009; Lee et al., 2008a; Zhao et al., 2016). ADI-15878 and ADI-15742 appear to bind distal to the β13-β14 loop (Figures 3B–3D and 3I).

The preceding findings suggested that ADI-15878 and ADI-15742 act primarily at a step that follows GP → GP_{CL} cleavage and receptor engagement. Because an endosomally generated GP_{CL} species (alone or in complex with NPC1) is the presumptive final target of these bNAbs, we examined the capacities of the base binders to neutralize VSV particles bearing GP_{CL} generated with CatL (Figures 5D, S5C, and S5G). Strikingly, GP cleavage enhanced the antiviral potencies of ADI-15946, ADI-15878, and ADI-15742 by 50- to 200-fold (not shown for ADI-15742), whereas it attenuated or eliminated neutralization by the other base binders tested.

Kinetic binding studies by biolayer interferometry (BLI) further elucidated pH- and cleavage-dependent changes in the apparent GP binding affinity of some NAbs (Figure 5E; Table S2). ADI-15878 bound with picomolar affinity to uncleaved GPΔTM at pH 7.5, but suffered a striking (10^3- to 10^4-fold) loss in apparent binding affinity at pH 5.5, the approximate pH of late endosomes. However, it regained picomolar binding affinity for CatL-cleaved GP_{CL}. ADI-15946 recognized uncleaved GPΔTM with nanomolar affinity at pH 7.5 and 5.5 and also gained picomolar binding to GP_{CL} at pH 5.5 (10^3- to 10^4-fold enhancement). Thus, the enhanced neutralization potential of these bNAbs against cleaved viruses may be at least partially attributable to improvements in GP binding. Interestingly, the monospecific base binders KZ52, c2G4, and c4G7 retained efficient binding to GP_{CL} despite their loss of neutralization against cleaved viruses, indicating that the nature of the epitope recognized, and not only binding affinity, dictates the molecular mechanism by which GP base-binding NAbs block ebolavirus entry.

Together, these results suggest that the bNAbs ADI-15878 and ADI-15742 differ from previously described monospecific base binders like KZ52, c2G4, c4G7, and mAb-100, in their capacity to target and neutralize a cleaved GP species that is generated deep in the endocytic pathway (Figure 5F). Conversely, the latter NAbs appear to act principally at and/or prior to the GP → GP_{CL} cleavage step. ADI-15946 displayed a dual behavior and may act both upstream, to block GP cleavage, and downstream, to target one or more GP_{CL}-like species at or near the membrane fusion step.

Germline Origin of ADI-15878 and ADI-15742 and Sequence Determinants of Their Neutralization Potency and Breadth

To begin to define the molecular basis of broad neutralization by ADI-15878 and ADI-15742, we assigned the V_H and V_L sequences of each bNAb to their respective germline genes and reverted ADI-15878 to its nearest inferred germline (IGL) precursor (Figure 6A). ADI-15878^{IGL} was engineered to contain germline reversions in most framework and complementarity-determining regions (CDR) segments but retain wild-type (WT) (fully mature) CDR-H3, because the originating germline sequence in this region could not be predicted with confidence given the highly diverse nature of D segments upon VDJ recombination. ADI-15878^{IGL} bound to EBOV GPΔTM (apparent

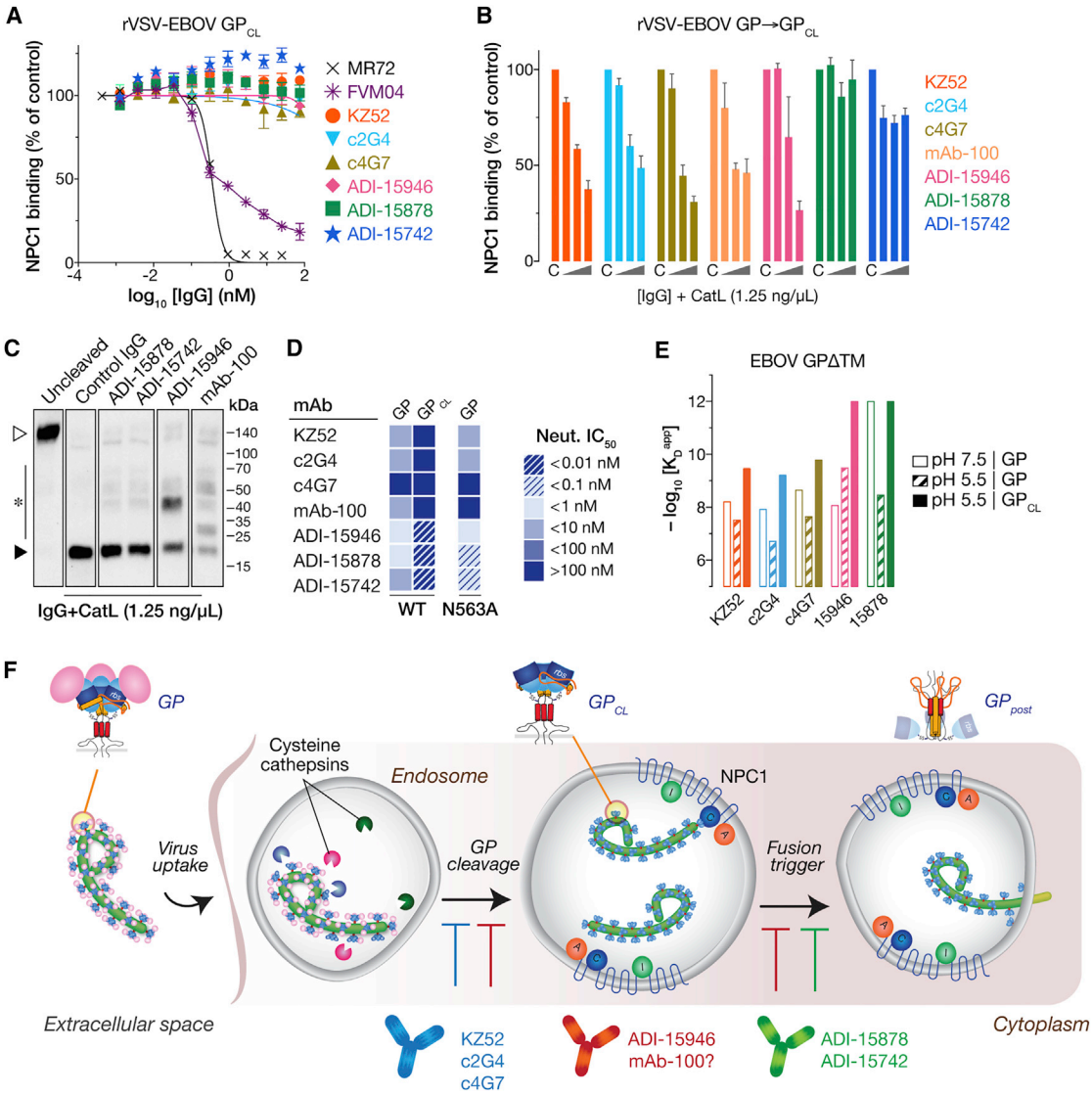

Figure 5. Mechanistic Basis of Human NAb-Dependent Blockade of Viral Entry

(A) Capacity of NAbs to block EBOV GP$_{CL}$:NPC1 binding in an ELISA. Immobilized rVSV-EBOV GP$_{CL}$ particles were incubated with increasing concentrations of each NAb and then with a pre-titrated concentration of purified NPC1 domain C-flag. Binding of NPC1 to GP$_{CL}$ was detected with an anti-flag antibody. Means ± SD for three replicates are shown.

(B) Capacity of NAbs to block exposure of the RBS mediated by GP → GP$_{CL}$ cleavage. rVSV-EBOV GP particles were incubated with cathepsin L (CatL) at pH 5.5 in the presence of increasing concentrations of each mAb. GP:NPC1 binding was detected by NPC1 ELISA as in (A). Means ± SD for six replicates from two pooled experiments are shown.

(C) Capacity of the NAbs to block EBOV GP → GP$_{CL}$ cleavage. Reactions from (B) were resolved by SDS-PAGE, and GP1 was visualized by western blotting. Open triangle, uncleaved GP1. Filled triangle, cleaved GP1. Asterisk, partially cleaved GP1 species. Blot image has been cropped to show only relevant lanes.

(D) Capacity of NAbs to neutralize viruses bearing uncleaved or cleaved GP (WT or N563A) in a single-round infection assay. Heatmaps of IC$_{50}$ values derived from NAb neutralization dose-curves of VSV-EBOV GP and CatL-generated VSV-EBOV GP$_{CL}$. Particles bearing EBOV GP(N563A) lack the conserved glycan at that residue. See also Figure S5.

(E) Kinetic binding constants and apparent binding affinities (K$_D^{app}$) for NAb:GP and NAb:GP$_{CL}$ interaction were determined by biolayer interferometry. See also Table S2.

(F) Schematic model for steps in ebolavirus entry targeted by NAbs.

K$_D$, K$_D^{app}$ ≈ 400 nM) by BLI) but lacked neutralizing activity (Figures 6B, 6C, S6, and S7). Heterodimeric light chain-heavy chain pairings containing one mature, somatic hypermutation (SHM)-bearing variable domain and one IGL variable domain bound to EBOV GP with single-digit nanomolar affinity (20- to 100-fold lower K$_D^{app}$), but picomolar affinity to EBOV GP required pairing of both mature chains (Figures S6A and S6C). The higher affinity of mature variable domains for binding to EBOV GP was

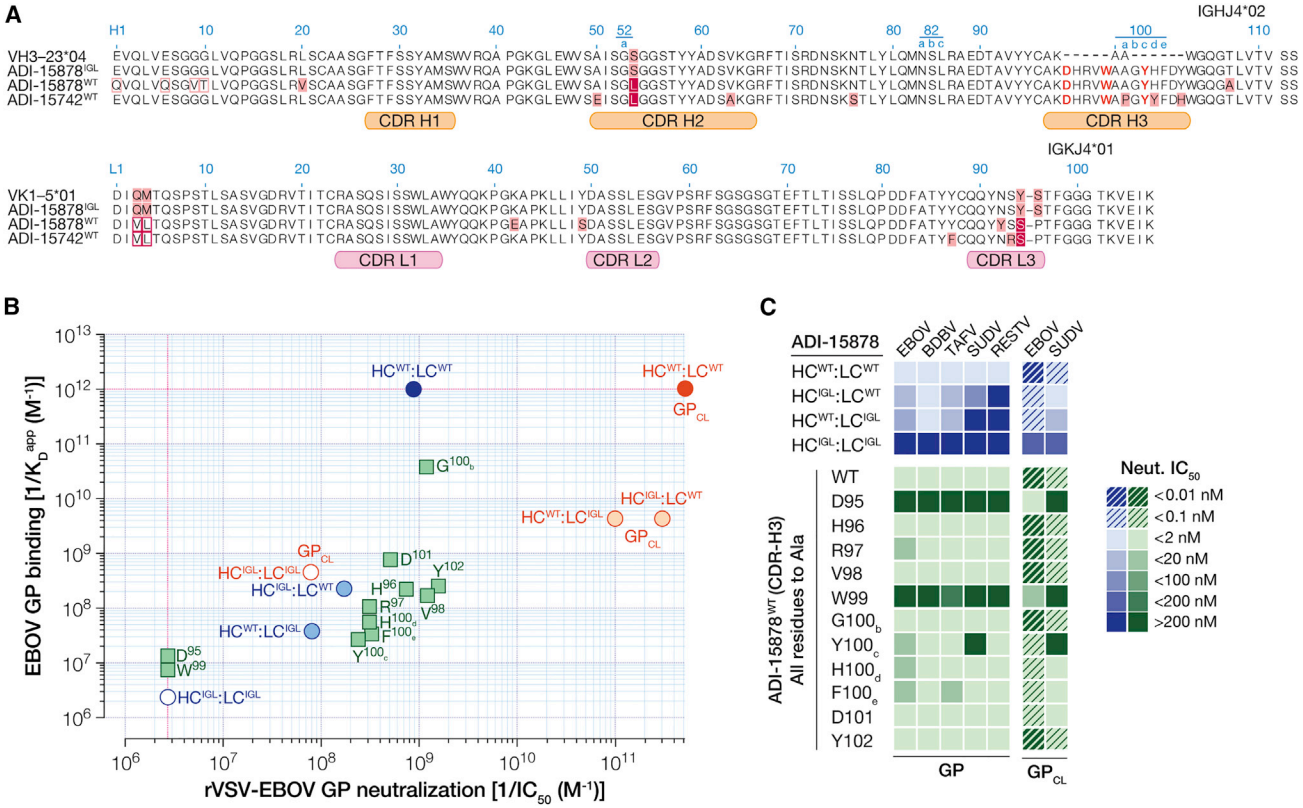

Figure 6. Germline Origin of ADI-15878 and Sequence Determinants of Its Neutralizing Activity

(A) Alignment of mature VH and VL sequences (ADI-15878^{WT} and ADI-15742^{WT}) with their closest human germline V and J gene segments and reconstruction of an inferred germline ancestor (ADI-15878^{IGL}) bearing mature CDR-H3 (Kabat numbering). Amino acid residues divergent from the inferred germline sequence are shaded in pink; substitutions shared by ADI-15878^{WT} and ADI-15742^{WT} are shaded in maroon. Open boxes, primer-induced mutations. CDR-H3 residues critical for viral neutralization are in red.

(B) Comparison of K_D^{app}s for NAb binding to GP and GP_{CL} versus neutralization of rVSV-EBOV GP infection (IC_{50}). Blue and orange circles, ADI-15878^{WT}, ADI-15878^{IGL}, and their HC:LC chimeras versus EBOV GP and GP_{CL}, respectively. Green squares, ADI-15878 bearing mutations in CDR-H3. Pink lines, high and low limits of detection for binding K_D^{app} and neutralization IC_{50}, respectively. See also (C) and Figures S5 and S6.

(C) Heatmaps for neutralization of rVSVs bearing ebolavirus GP and GP_{CL} by ADI-15878 variants. See also (B) and Figure S6.

See also Figure S7.

primarily due to slower dissociation rates (k_{off}) relative to variants containing one or both IGL segments. These changes in binding affinity associated with variable region maturation were accompanied by incremental improvements in neutralization potency and breadth. However, neutralization of rVSVs bearing SUDV and RESTV GP was especially dependent on sequences containing light chain SHMs, indicating a critical role for ADI-15878 light chain:GP interactions in neutralization breadth (Figures 6C and S7). Together, these findings suggest that the CDRs of both V_H (non-CDR-H3) and V_L sequences of ADI-15878 and ADI-15742 make key contributions to the energetics of ebolavirus GP binding and to pan-ebolavirus neutralizing efficacy.

To complement the above analysis, we separately assessed the contributions of individual CDR-H3 residues in ADI-15878 by alanine scanning mutagenesis (Figures 6B, 6C, S6, and S7). WT ADI-15878 mAb exhibited a slow off rate for both GP and GP_{CL} (below the 10^{-7} s^{-1} detection limit of BLI, providing a <1 pM estimate of K_D^{app}). Most of the WT → Ala CDR-H3 mutants exhibited dramatically lower binding to EBOV GP (K_D^{app}s 20- to 74,000-fold higher than 1 pM), indicating that mutations were either detrimental to direct binding interactions or altered productive CDR-H3 loop conformations. However, all of the WT → Ala CDR-H3 mutants had only modest effects on neutralization potency against rVSV-EBOV GP relative to WT ADI-15878, except D95A and W99A, which suffered an ≈99% reduction in potency. The impact on neutralization of each CDR-H3 mutant, including D95A and W99A, was even less pronounced against rVSV-EBOV GP_{CL} (Figures 6C and S7), consistent with enhanced mAb:GP_{CL} binding affinity and GP_{CL} neutralization sensitivity (Figure 6B; Table S2). These neutralization trends extended to GPs from the other ebolaviruses, except for $Y100_cA$, which was selectively less potent against rVSVs bearing SUDV GP and GP_{CL} (Figures 6C, S7C, and S7D). These results suggest that interactions between the CDR-H3 loop of ADI-15878 and structurally conserved elements in the GP2 IFL and HR1 contribute to pan-ebolavirus recognition and neutralization. Furthermore, they identify three WT side chains (D95,

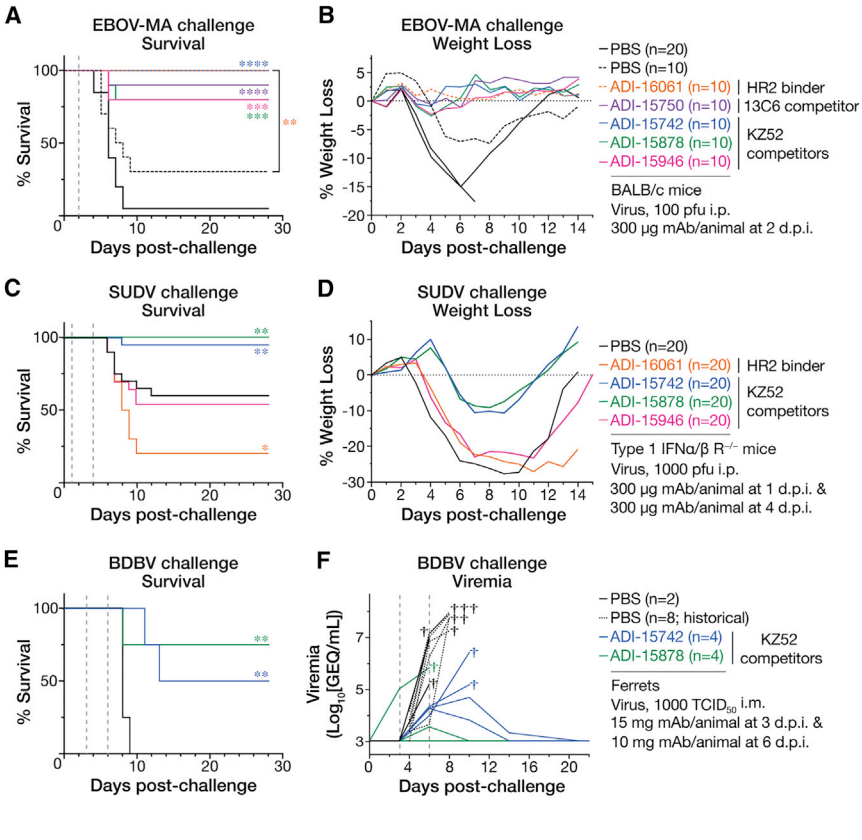

Figure 7. In Vivo Protective Efficacy of Broadly Neutralizing Human mAbs

(A) BALB/c mice were challenged with mouse-adapted EBOV (EBOV-MA) and then treated with a single dose of each NAb or vehicle (PBS).

(B) Weight loss curves for control and NAb-treated groups in (A).

(C) Type 1 IFNα/β $R^{-/-}$ mice were challenged with WT SUDV and then treated with two doses of each NAb or PBS.

(D) Weight loss curves for control and NAb-treated groups in (C).

(E) Ferrets were challenged with WT BDBV and then treated with two doses of each NAb or PBS.

(F) Measurements of plasma viremia in infected ferrets in (E) (GEQ, viral genome equivalents). †, deceased animal. See also Table S3.

n, number of animals per group. *$p < 0.05$; **$p < 0.01$; ***$p < 0.001$; ****$p < 0.0001$. All other comparisons to the PBS group were not significant.

W99, $Y100_c$) that are critical to the pan-ebolavirus neutralizing activity of ADI-15878.

Protective Efficacy in Animal Models of EBOV, SUDV, and BDBV Challenge

We assessed the protective efficacy of the human bNAbs in three small-animal models of lethal ebolavirus challenge (Figure 7). First, wild-type (WT) BALB/c mice were exposed to mouse-adapted EBOV (EBOV-MA) and then administered a single dose of each bNAb at 2 days post-infection (Figures 7A and 7B). bNAbs from each epitope group were highly (≥80%) protective against EBOV in this stringent post-exposure setting with little or no weight loss apparent in antibody-treated animals.

We next evaluated the bNAbs in the type I interferon α/β receptor-deficient mouse model for SUDV challenge (Figures 7C and 7D) (Brannan et al., 2015). Mice were exposed to WT SUDV and then dosed with each bNAb on days 1 and 4 post-infection. ADI-15878 and ADI-15742 afforded ≥95% survival and greatly reduced weight loss, relative to the PBS vehicle group. By contrast, ADI-16061 and ADI-15946, both weak SUDV neutralizers, provided little or no protection. To the contrary, ADI-16061 significantly increased mortality in two independent experiments ($p < 0.05$), raising the possibility that it can enhance SUDV infection in vivo.

Finally, we tested the anti-BDBV efficacy of the two pan-ebolavirus bNAbs, ADI-15878 and ADI-15742, in the domestic ferret, which is the only described non-NHP model for BDBV challenge (Figures 7E and 7F) (Cross et al., 2016; Kozak et al., 2016). Animals received two doses of each bNAb. As observed previously (Cross et al., 2016; Kozak et al., 2016), BDBV infection was uniformly lethal, with PBS-treated animals succumbing between days 8–10 following challenge. By contrast, both bNAbs afforded highly significant levels of survival ($p < 0.01$; three of four animals for ADI-15878; two of four for ADI-15742). Furthermore, peak viremia levels correlated with bNAb treatment and survival outcome, with lower viral titers observed in the surviving animals relative to those that succumbed to infection ($p = 0.0011$) and in bNAb-treated animals relative to PBS-treated controls ($p = 0.0006$). Viremia also trended lower in animals receiving ADI-15878 relative to those receiving ADI-15742, but this difference did not reach statistical significance. Strikingly, analysis of the BDBV GP consensus sequence in blood samples collected from viremic animals at day 6 post-challenge revealed a single nucleotide change encoding the G528S mutation in all four of the ADI-15742-treated animals, but in none of the ADI-15878-treated and PBS-treated animals for which viral RNA could be isolated (Table S3). Mutation of the same GP2 IFL residue conferred viral neutralization escape from both antibodies in tissue culture (Figures 3, S2, and S3). These results raise the possibility that ADI-15878 engenders viral neutralization escape to a lesser extent than ADI-15742 in vivo and suggests that ADI-15878 should be prioritized over ADI-15742 as a component of a pan-ebolavirus immunotherapeutic.

In sum, our findings demonstrate that the pan-ebolavirus bNAbs ADI-15878 and ADI-15742 can afford post-exposure protection against challenge by the three divergent ebolaviruses currently associated with lethal disease outbreaks in humans.

DISCUSSION

Herein, we identified bNAbs from a human survivor of the 2013–2016 West African EBOV epidemic, including two with potent

pan-ebolavirus neutralizing activity. Flyak et al. (2016) previously reported a bNAb, BDBV43, from a survivor of BDBV infection, but two features limit its therapeutic utility in comparison to the human bNAbs described in this study. First, BDBV43 neutralizes EBOV, BDBV, and SUDV weakly (IC_{50} >100 nM). Second, BDBV43, a glycan cap binder, cross-reacts with the secreted form of the glycoprotein (sGP). sGP is present at high levels in EVD patients (Sanchez et al., 1996) and may "soak up" mAbs that recognize it (Mohan et al., 2012) potentially reducing their capacity to target and neutralize infectious virions.

We uncovered cross-neutralizing mAbs that not only target the glycan cap and sGP (ADI-15750) (Bornholdt et al., 2016b) but also other structural regions of the trimeric GP spike, namely the base and internal fusion loop (IFL) (ADI-15878, ADI-15742, ADI-15946) and the stalk (ADI-16061). The broadest and most potent of these bNAbs recognize base epitopes. ADI-15878 and ADI-15742, two clonally related mAbs of the 349 screened, afforded highly potent neutralizing activity (IC_{50} <1 nM) against all five known ebolaviruses. A third base binder, ADI-15946, could potently neutralize four of five ebolaviruses (except RESTV) but demonstrated only modest activity against SUDV.

Our findings reveal unusual modes of neutralization by ADI-15878, ADI-15742, and ADI-15946. Specifically, ADI-15878 and ADI-15742 appear to target a cleaved GP intermediate in endosomes, whereas the prototypic base binders KZ52, c2G4, and c4G7 act only at one or more upstream steps in entry, as also proposed by Misasi et al. (2016) (Figures 5F, S5A, and S5B). The protomer-spanning mode of ADI-15878/15742 binding is predicted to "lock" the cleaved GP trimer, whether free or bound to NPC1, in a pre-fusion state, thereby arresting GP conformational changes required for viral membrane fusion. ADI-15946 appears to act at both upstream and downstream entry steps and may arrest the transduction of receptor-induced conformational changes required for fusion by binding GP1 residues adjacent to the RBS (71–77) (Figures 4F and S3D). These residues were shown to rearrange upon GP_{CL}:NPC1 association (Wang et al., 2016). The prototypic base binders do not appear to make such GP1 contacts (Figures 4G and 4H).

To explore the genesis of pan-ebolavirus bNAbs in humans infected with a single ebolavirus, we characterized "germline-reverted" variants of ADI-15878 for viral binding and neutralization. Our results suggest that, although ADI-15878/15742-like pan-ebolavirus neutralizing mAbs did not arise with high frequency in this human survivor of EVD (2/349), the barrier for maturation of such mAbs may be lower than that seen in some other viral diseases. ADI-15878 and ADI-15742 originate from the most common germline heavy chain segment (VH3-23), do not possess extremely long CDR-H3s (15 amino acids versus 20–33 for HIV-1-specific bNAbs whose epitopes contain protein sequences and glycans), and require only a few SHMs for broad and potent antiviral activity (≈6% amino acid changes in V_H versus ≈30% for HIV-1 CD4-binding site-specific bNAbs) (Bornholdt et al., 2016b; Corti and Lanzavecchia, 2013; Tiller et al., 2013). Furthermore, a germline-reverted variant of ADI-15878 (albeit with a mature CDR-H3) could recognize EBOV GP with submicromolar affinity (Figures 6 and S6). The presence of bNAbs in polyclonal primary responses to ebolavirus infection contrasts with the origin of such bNAbs in human subjects who control long-term HIV-1 infection or with active secondary dengue virus infection (Corti and Lanzavecchia, 2013; Dejnirattisai et al., 2015).

Our findings further suggest the possibility of eliciting anti-ebolavirus bNAbs efficiently in humans through immunization with a suitably engineered immunogen, because the sites of broad vulnerability within GP are clearly defined, and the generation of ADI-15878-like responses requires only subtle maturation of an abundantly represented germline. Strikingly, the germline-reverted ADI-15878 variant could bind to soluble EBOV GP_{CL} with single-digit nanomolar K_D^{app} and neutralize viruses bearing EBOV and SUDV GP_{CL} (Figures 6C, S6A, and S7A). Thus, minimized EBOV GP constructs mimicking GP_{CL} may preferentially elicit ADI-15878-like antibodies through enhanced presentation of vulnerable IFL epitopes, increased activation of the appropriate B cell precursors, and removal of putatively immunodominant and generally non-neutralizing epitopes in the glycan cap and mucin domain. Such germline-targeting immunogens could be further improved by modification of the GP glycan landscape (e.g., at residue 563) and may have utility as part of a broadly protective next-generation filovirus vaccine.

ADI-15878 and ADI-15742 protect against EBOV, BDBV, and SUDV in vivo under stringent post-exposure conditions when administered as monotherapy, and our results suggest that they should also afford protection against all other known ebolaviruses. By contrast, the ZMapp cocktail, which represents the current state-of-the-art for anti-filovirus immunotherapy, is only efficacious against a single virus, EBOV. Moreover, ZMapp component c13C6 cross-reacts with sGP, and all three mAbs lack activity against endosomally cleaved forms of GP. Next-generation cocktails comprising bNAbs like ADI-15878, ADI-15946, and/or CA45 (Zhao et al., 2017; this issue of *Cell*), which elude subversion by sGP (Bornholdt et al., 2016b) and can act synergistically to block both uncleaved and cleaved forms of GP (Figure 5F), should provide broad protection at significantly lower doses, while reducing the risk of neutralization escape that is inherent to antibody monotherapy.

STAR★METHODS

Detailed methods are provided in the online version of this paper and include the following:

- KEY RESOURCES TABLE
- CONTACT FOR REAGENT AND RESOURCE SHARING
- EXPERIMENTAL MODEL AND SUBJECT DETAILS
  - Cell lines
  - Vesicular stomatitis virus (VSV) recombinants and pseudotypes
  - Authentic filoviruses
- METHOD DETAILS
  - Generation of cleaved VSV-GP particles and GPΔTM ectodomain proteins
  - VSV infectivity measurements and neutralization assays
  - Authentic filovirus microneutralization assays
  - Generation of mAbs
  - ELISAs for GP:mAb binding

- Competition ELISAs for GP/mAb binding to NPC1
- ELISAs and immunoblots to detect mAb inhibition of GP cleavage
- Selection of viral neutralization escape mutants
- Single-particle electron microscopy
- Structural representation of ebolavirus GP sequence conservation
- GP:mAb kinetic binding analysis by biolayer interferometry (BLI)
- EBOV and SUDV challenge studies in mice
- BDBV challenge studies in ferrets
- BDBV GP sequencing from ferret blood samples
- Animal welfare statement

● QUANTIFICATION AND STATISTICAL ANALYSIS

● DATA AND SOFTWARE AVAILABILITY

SUPPLEMENTAL INFORMATION

Supplemental Information includes seven figures and three tables and can be found with this article online at http://dx.doi.org/10.1016/j.cell.2017.04.037.

AUTHOR CONTRIBUTIONS

A.Z.W., A.S.H., C.D.M., E.K.N., D.M.A., J.M.F., S.H., R.M.J., M.-A.d.L.V., W.Z., R.R.B., E.G., H.L.T., L.Z., R.K.J., X.Q., J.R.L., L.M.W., A.B.W., J.M.D., K.C., and Z.A.B. designed research, analyzed data, and wrote and/or edited the paper. E.G. and L.M.W. designed the germline-reverted constructs. E.G., L.M.W., A.Z.W., D.M.A., and Z.A.B. produced GPs and mAbs for structural and functional studies. A.Z.W., E.K.N., J.M.F., R.K.J., D.M.A., and Z.A.B. characterized the binding, neutralization, and other functional properties of the mAbs. C.D.M., H.L.T., and A.B.W. performed structural studies on GP:Fab complexes. A.S.H., R.M.J., and R.R.B. performed the mouse challenge studies. S.H., M.-A.d.L.V., W.Z., and X.Q. performed the ferret challenge studies. Z.A.B. and D.M.A. are employees of Mapp Biopharmaceutical. L.Z. is an employee, shareholder, and owner of Mapp Biopharmaceutical. E.G. and L.W. are employees and shareholders of Adimab.

ACKNOWLEDGMENTS

We thank C. Harold, T. Alkutkar, and T.B. Krause for technical assistance. Support for this work was provided by NIH grants U19 AI109762 (Centers for Excellence in Translational Research) to K.C., J.R.L., J.M.D., A.B.W., and L.Z., DTRA contract HDTRA1-13-C-0018 to L.Z., D.M.A., and Z.A.B., and DTRA contract CB4077 to A.S.H., R.R.B., R.M.J., and J.M.D. This work was also supported by Public Health Agency of Canada. E.K.N. was also supported by a DAAD (Deutscher Akademischer Austauschdienst, German Academic Exchange Service) fellowship.

Received: December 20, 2016
Revised: March 16, 2017
Accepted: April 26, 2017
Published: May 18, 2017

REFERENCES

Audet, J., Wong, G., Wang, H., Lu, G., Gao, G.F., Kobinger, G., and Qiu, X. (2014). Molecular characterization of the monoclonal antibodies composing ZMAb: a protective cocktail against Ebola virus. Sci. Rep. *4*, 6881.

Bornholdt, Z.A., Ndungo, E., Fusco, M.L., Bale, S., Flyak, A.I., Crowe, J.E., Jr., Chandran, K., and Saphire, E.O. (2016a). Host-primed Ebola virus GP exposes a hydrophobic NPC1 receptor-binding pocket, revealing a target for broadly neutralizing antibodies. MBio *7*, e02154–e15.

Bornholdt, Z.A., Turner, H.L., Murin, C.D., Li, W., Sok, D., Souders, C.A., Piper, A.E., Goff, A., Shamblin, J.D., Wollen, S.E., et al. (2016b). Isolation of potent neutralizing antibodies from a survivor of the 2014 Ebola virus outbreak. Science *351*, 1078–1083.

Brannan, J.M., Froude, J.W., Prugar, L.I., Bakken, R.R., Zak, S.E., Daye, S.P., Wilhelmsen, C.E., and Dye, J.M. (2015). Interferon α/β receptor-deficient mice as a model for Ebola virus disease. J. Infect. Dis. *212* (*Suppl 2*), S282–S294.

Bray, M., Davis, K., Geisbert, T., Schmaljohn, C., and Huggins, J. (1998). A mouse model for evaluation of prophylaxis and therapy of Ebola hemorrhagic fever. J. Infect. Dis. *178*, 651–661.

Brecher, M., Schornberg, K.L., Delos, S.E., Fusco, M.L., Saphire, E.O., and White, J.M. (2012). Cathepsin cleavage potentiates the Ebola virus glycoprotein to undergo a subsequent fusion-relevant conformational change. J. Virol. *86*, 364–372.

Burk, R., Bollinger, L., Johnson, J.C., Wada, J., Radoshitzky, S.R., Palacios, G., Bavari, S., Jahrling, P.B., and Kuhn, J.H. (2016). Neglected filoviruses. FEMS Microbiol. Rev. *40*, 494–519.

Carette, J.E., Raaben, M., Wong, A.C., Herbert, A.S., Obernosterer, G., Mulherkar, N., Kuehne, A.I., Kranzusch, P.J., Griffin, A.M., Ruthel, G., et al. (2011). Ebola virus entry requires the cholesterol transporter Niemann-Pick C1. Nature *477*, 340–343.

Chandran, K., Sullivan, N.J., Felbor, U., Whelan, S.P., and Cunningham, J.M. (2005). Endosomal proteolysis of the Ebola virus glycoprotein is necessary for infection. Science *308*, 1643–1645.

Clark, J.D., Gebhart, G.F., Gonder, J.C., Keeling, M.E., and Kohn, D.F. (1997). The 1996 Guide for the Care and Use of Laboratory Animals. ILAR J *38*, 41–48.

Corti, D., and Lanzavecchia, A. (2013). Broadly neutralizing antiviral antibodies. Annu. Rev. Immunol. *31*, 705–742.

Côté, M., Misasi, J., Ren, T., Bruchez, A., Lee, K., Filone, C.M., Hensley, L., Li, Q., Ory, D., Chandran, K., and Cunningham, J. (2011). Small molecule inhibitors reveal Niemann-Pick C1 is essential for Ebola virus infection. Nature *477*, 344–348.

Cross, R.W., Mire, C.E., Borisevich, V., Geisbert, J.B., Fenton, K.A., and Geisbert, T.W. (2016). The domestic ferret (Mustela putorius furo) as a lethal infection model for 3 species of Ebolavirus. J. Infect. Dis. *214*, 565–569.

Davey, R.T., Jr., Dodd, L., Proschan, M.A., Neaton, J., Neuhaus Nordwall, J., Koopmeiners, J.S., Beigel, J., Tierney, J., Lane, H.C., Fauci, A.S., et al.; PREVAIL II Writing Group; Multi-National PREVAIL II Study Team (2016). A randomized, controlled trial of ZMapp for Ebola virus infection. N. Engl. J. Med. *375*, 1448–1456.

de La Vega, M.A., Stein, D., and Kobinger, G.P. (2015). Ebolavirus evolution: past and present. PLoS Pathog. *11*, e1005221.

Dejnirattisai, W., Wongwiwat, W., Supasa, S., Zhang, X., Dai, X., Rouvinski, A., Jumnainsong, A., Edwards, C., Quyen, N.T., Duangchinda, T., et al. (2015). A new class of highly potent, broadly neutralizing antibodies isolated from viremic patients infected with dengue virus. Nat. Immunol. *16*, 170–177.

Dias, J.M., Kuehne, A.I., Abelson, D.M., Bale, S., Wong, A.C., Halfmann, P., Muhammad, M.A., Fusco, M.L., Zak, S.E., Kang, E., et al. (2011). A shared structural solution for neutralizing ebolaviruses. Nat. Struct. Mol. Biol. *18*, 1424–1427.

Dube, D., Brecher, M.B., Delos, S.E., Rose, S.C., Park, E.W., Schornberg, K.L., Kuhn, J.H., and White, J.M. (2009). The primed ebolavirus glycoprotein (19-kilodalton GP1,2): sequence and residues critical for host cell binding. J. Virol. *83*, 2883–2891.

WHO International Study Team (1978). Ebola haemorrhagic fever in Sudan, 1976. Bull. World Health Organ. *56*, 247–270.

Flyak, A.I., Ilinykh, P.A., Murin, C.D., Garron, T., Shen, X., Fusco, M.L., Hashiguchi, T., Bornholdt, Z.A., Slaughter, J.C., Sapparapu, G., et al. (2015). Mechanism of human antibody-mediated neutralization of Marburg virus. Cell *160*, 893–903.

Flyak, A.I., Shen, X., Murin, C.D., Turner, H.L., David, J.A., Fusco, M.L., Lampley, R., Kose, N., Ilinykh, P.A., Kuzmina, N., et al. (2016). Cross-reactive and potent neutralizing antibody responses in human survivors of natural Ebolavirus infection. Cell *164*, 392–405.

Frei, J.C., Nyakatura, E.K., Zak, S.E., Bakken, R.R., Chandran, K., Dye, J.M., and Lai, J.R. (2016). Bispecific antibody affords complete post-exposure protection of mice from both Ebola (Zaire) and Sudan viruses. Sci. Rep. *6*, 19193.

Furuyama, W., Marzi, A., Nanbo, A., Haddock, E., Maruyama, J., Miyamoto, H., Igarashi, M., Yoshida, R., Noyori, O., Feldmann, H., and Takada, A. (2016). Discovery of an antibody for pan-ebolavirus therapy. Sci. Rep. *6*, 20514.

Goddard, T.D., Huang, C.C., and Ferrin, T.E. (2007). Visualizing density maps with UCSF Chimera. J. Struct. Biol. *157*, 281–287.

Holtsberg, F.W., Shulenin, S., Vu, H., Howell, K.A., Patel, S.J., Gunn, B., Karim, M., Lai, J.R., Frei, J.C., Nyakatura, E.K., et al. (2015). Pan-ebolavirus and Pan-filovirus mouse monoclonal antibodies: protection against Ebola and Sudan viruses. J. Virol. *90*, 266–278.

Howell, K.A., Qiu, X., Brannan, J.M., Bryan, C., Davidson, E., Holtsberg, F.W., Wec, A.Z., Shulenin, S., Biggins, J.E., Douglas, R., et al. (2016). Antibody treatment of Ebola and Sudan virus infection via a uniquely exposed epitope within the glycoprotein receptor-binding site. Cell Rep. *15*, 1514–1526.

Jahrling, P.B., Geisbert, T.W., Geisbert, J.B., Swearengen, J.R., Bray, M., Jaax, N.K., Huggins, J.W., LeDuc, J.W., and Peters, C.J. (1999). Evaluation of immune globulin and recombinant interferon-alpha2b for treatment of experimental Ebola virus infections. J. Infect. Dis. *179* (*Suppl 1*), S224–S234.

Keck, Z.Y., Enterlein, S.G., Howell, K.A., Vu, H., Shulenin, S., Warfield, K.L., Froude, J.W., Araghi, N., Douglas, R., Biggins, J., et al. (2015). Macaque monoclonal antibodies targeting novel conserved epitopes within filovirus glycoprotein. J. Virol. *90*, 279–291.

Kozak, R., He, S., Kroeker, A., de La Vega, M.A., Audet, J., Wong, G., Urfano, C., Antonation, K., Embury-Hyatt, C., Kobinger, G.P., and Qiu, X. (2016). Ferrets infected with Bundibugyo virus or Ebola virus recapitulate important aspects of human filovirus disease. J. Virol. *90*, 9209–9223.

Kuhn, J.H., Andersen, K.G., Baize, S., Bào, Y., Bavari, S., Berthet, N., Blinkova, O., Brister, J.R., Clawson, A.N., Fair, J., et al. (2014). Nomenclature- and database-compatible names for the two Ebola virus variants that emerged in Guinea and the Democratic Republic of the Congo in 2014. Viruses *6*, 4760–4799.

Lander, G.C., Stagg, S.M., Voss, N.R., Cheng, A., Fellmann, D., Pulokas, J., Yoshioka, C., Irving, C., Mulder, A., Lau, P.W., et al. (2009). Appion: an integrated, database-driven pipeline to facilitate EM image processing. J. Struct. Biol. *166*, 95–102.

Larkin, M.A., Blackshields, G., Brown, N.P., Chenna, R., McGettigan, P.A., McWilliam, H., Valentin, F., Wallace, I.M., Wilm, A., Lopez, R., et al. (2007). Clustal W and Clustal X version 2.0. Bioinformatics *23*, 2947–2948.

Lee, J.E., Fusco, M.L., Hessell, A.J., Oswald, W.B., Burton, D.R., and Saphire, E.O. (2008a). Structure of the Ebola virus glycoprotein bound to an antibody from a human survivor. Nature *454*, 177–182.

Lee, J.E., Kuehne, A., Abelson, D.M., Fusco, M.L., Hart, M.K., and Saphire, E.O. (2008b). Complex of a protective antibody with its Ebola virus GP peptide epitope: unusual features of a V lambda x light chain. J. Mol. Biol. *375*, 202–216.

Macneil, A., Reed, Z., and Rollin, P.E. (2011). Serologic cross-reactivity of human IgM and IgG antibodies to five species of Ebola virus. PLoS Negl. Trop. Dis. *5*, e1175.

Maruyama, T., Rodriguez, L.L., Jahrling, P.B., Sanchez, A., Khan, A.S., Nichol, S.T., Peters, C.J., Parren, P.W., and Burton, D.R. (1999). Ebola virus can be effectively neutralized by antibody produced in natural human infection. J. Virol. *73*, 6024–6030.

Miller, E.H., and Chandran, K. (2012). Filovirus entry into cells - new insights. Curr. Opin. Virol. *2*, 206–214.

Miller, E.H., Obernosterer, G., Raaben, M., Herbert, A.S., Deffieu, M.S., Krishnan, A., Ndungo, E., Sandesara, R.G., Carette, J.E., Kuehne, A.I., et al. (2012). Ebola virus entry requires the host-programmed recognition of an intracellular receptor. EMBO J. *31*, 1947–1960.

Misasi, J., Chandran, K., Yang, J.Y., Considine, B., Filone, C.M., Côté, M., Sullivan, N., Fabozzi, G., Hensley, L., and Cunningham, J. (2012). Filoviruses require endosomal cysteine proteases for entry but exhibit distinct protease preferences. J. Virol. *86*, 3284–3292.

Misasi, J., Gilman, M.S., Kanekiyo, M., Gui, M., Cagigi, A., Mulangu, S., Corti, D., Ledgerwood, J.E., Lanzavecchia, A., Cunningham, J., et al. (2016). Structural and molecular basis for Ebola virus neutralization by protective human antibodies. Science *351*, 1343–1346.

Mohan, G.S., Li, W., Ye, L., Compans, R.W., and Yang, C. (2012). Antigenic subversion: a novel mechanism of host immune evasion by Ebola virus. PLoS Pathog. *8*, e1003065.

Moller-Tank, S., and Maury, W. (2015). Ebola virus entry: a curious and complex series of events. PLoS Pathog. *11*, e1004731.

Murin, C.D., Fusco, M.L., Bornholdt, Z.A., Qiu, X., Olinger, G.G., Zeitlin, L., Kobinger, G.P., Ward, A.B., and Saphire, E.O. (2014). Structures of protective antibodies reveal sites of vulnerability on Ebola virus. Proc. Natl. Acad. Sci. USA *111*, 17182–17187.

Natesan, M., Jensen, S.M., Keasey, S.L., Kamata, T., Kuehne, A.I., Stonier, S.W., Lutwama, J.J., Lobel, L., Dye, J.M., and Ulrich, R.G. (2016). Human survivors of disease outbreaks caused by Ebola or Marburg virus exhibit cross-reactive and long-lived antibody responses. Clin. Vaccine Immunol. *23*, 717–724.

National Research Council (2011). Guide for the Care and Use of Laboratory Animals, Eighth Edition (National Academies Press).

Ng, M., Ndungo, E., Jangra, R.K., Cai, Y., Postnikova, E., Radoshitzky, S.R., Dye, J.M., Ramírez de Arellano, E., Negredo, A., Palacios, G., et al. (2014). Cell entry by a novel European filovirus requires host endosomal cysteine proteases and Niemann-Pick C1. Virology *468-470*, 637–646.

Ogura, T., Iwasaki, K., and Sato, C. (2003). Topology representing network enables highly accurate classification of protein images taken by cryo electron-microscope without masking. J. Struct. Biol. *143*, 185–200.

Pallesen, J., Murin, C.D., de Val, N., Cottrell, C.A., Hastie, K.M., Turner, H.L., Fusco, M.L., Flyak, A.I., Zeitlin, L., Crowe, J.E., Jr., et al. (2016). Structures of Ebola virus GP and sGP in complex with therapeutic antibodies. Nat. Microbiol. *1*, 16128.

Pei, J., and Grishin, N.V. (2001). AL2CO: calculation of positional conservation in a protein sequence alignment. Bioinformatics *17*, 700–712.

Pettersen, E.F., Goddard, T.D., Huang, C.C., Couch, G.S., Greenblatt, D.M., Meng, E.C., and Ferrin, T.E. (2004). UCSF Chimera–a visualization system for exploratory research and analysis. J. Comput. Chem. *25*, 1605–1612.

Qiu, X., Wong, G., Audet, J., Bello, A., Fernando, L., Alimonti, J.B., Fausther-Bovendo, H., Wei, H., Aviles, J., Hiatt, E., et al. (2014). Reversion of advanced Ebola virus disease in nonhuman primates with ZMapp. Nature *514*, 47–53.

Sanchez, A., Trappier, S.G., Mahy, B.W., Peters, C.J., and Nichol, S.T. (1996). The virion glycoproteins of Ebola viruses are encoded in two reading frames and are expressed through transcriptional editing. Proc. Natl. Acad. Sci. USA *93*, 3602–3607.

Schornberg, K., Matsuyama, S., Kabsch, K., Delos, S., Bouton, A., and White, J. (2006). Role of endosomal cathepsins in entry mediated by the Ebola virus glycoprotein. J. Virol. *80*, 4174–4178.

Shedlock, D.J., Bailey, M.A., Popernack, P.M., Cunningham, J.M., Burton, D.R., and Sullivan, N.J. (2010). Antibody-mediated neutralization of Ebola virus can occur by two distinct mechanisms. Virology *401*, 228–235.

Simmons, J.A., D'Souza, R.S., Ruas, M., Galione, A., Casanova, J.E., and White, J.M. (2015). Ebolavirus glycoprotein directs fusion through NPC1+ endolysosomes. J. Virol. *90*, 605–610.

Spence, J.S., Krause, T.B., Mittler, E., Jangra, R.K., and Chandran, K. (2016). Direct visualization of Ebola virus fusion triggering in the endocytic pathway. MBio *7*, e01857–e15.

Suloway, C., Pulokas, J., Fellmann, D., Cheng, A., Guerra, F., Quispe, J., Stagg, S., Potter, C.S., and Carragher, B. (2005). Automated molecular microscopy: the new Leginon system. J. Struct. Biol. *151*, 41–60.

Takada, A., Robison, C., Goto, H., Sanchez, A., Murti, K.G., Whitt, M.A., and Kawaoka, Y. (1997). A system for functional analysis of Ebola virus glycoprotein. Proc. Natl. Acad. Sci. USA *94*, 14764–14769.

Tang, G., Peng, L., Baldwin, P.R., Mann, D.S., Jiang, W., Rees, I., and Ludtke, S.J. (2007). EMAN2: an extensible image processing suite for electron microscopy. J. Struct. Biol. *157*, 38–46.

Tiller, T., Schuster, I., Deppe, D., Siegers, K., Strohner, R., Herrmann, T., Berenguer, M., Poujol, D., Stehle, J., Stark, Y., et al. (2013). A fully synthetic human Fab antibody library based on fixed VH/VL framework pairings with favorable biophysical properties. MAbs *5*, 445–470.

Towner, J.S., Sealy, T.K., Khristova, M.L., Albariño, C.G., Conlan, S., Reeder, S.A., Quan, P.L., Lipkin, W.I., Downing, R., Tappero, J.W., et al. (2008). Newly discovered ebola virus associated with hemorrhagic fever outbreak in Uganda. PLoS Pathog. *4*, e1000212.

Voss, N.R., Yoshioka, C.K., Radermacher, M., Potter, C.S., and Carragher, B. (2009). DoG Picker and TiltPicker: software tools to facilitate particle selection in single particle electron microscopy. J. Struct. Biol. *166*, 205–213.

Wang, H., Shi, Y., Song, J., Qi, J., Lu, G., Yan, J., and Gao, G.F. (2016). Ebola viral glycoprotein bound to its endosomal receptor Niemann-Pick C1. Cell *164*, 258–268.

Wec, A.Z., Nyakatura, E.K., Herbert, A.S., Howell, K.A., Holtsberg, F.W., Bakken, R.R., Mittler, E., Christin, J.R., Shulenin, S., Jangra, R.K., et al. (2016). A "Trojan horse" bispecific-antibody strategy for broad protection against ebolaviruses. Science *354*, 350–354.

Wong, G., and Kobinger, G.P. (2015). Backs against the wall: novel and existing strategies used during the 2014-2015 Ebola virus outbreak. Clin. Microbiol. Rev. *28*, 593–601.

Wong, A.C., Sandesara, R.G., Mulherkar, N., Whelan, S.P., and Chandran, K. (2010). A forward genetic strategy reveals destabilizing mutations in the Ebolavirus glycoprotein that alter its protease dependence during cell entry. J. Virol. *84*, 163–175.

Zhao, Y., Ren, J., Harlos, K., Jones, D.M., Zeltina, A., Bowden, T.A., Padilla-Parra, S., Fry, E.E., and Stuart, D.I. (2016). Toremifene interacts with and destabilizes the Ebola virus glycoprotein. Nature *535*, 169–172.

Zhao, X., Howell, K.A., He, S., Brannan, J.M., Wec, A.Z., Davidson, E., Turner, H.L., Chiang, C.-I., Lei, L., Fels, J.M., et al. (2017). Immunization-elicited broadly protective antibody reveals ebolavirus fusion loop as a site of vulnerability. Cell *169*, this issue, ■■■–■■■.

Please cite this article in press as: Wec et al., Antibodies from a Human Survivor Define Sites of Vulnerability for Broad Protection against Ebolaviruses, Cell (2017), http://dx.doi.org/10.1016/j.cell.2017.04.037

STAR★METHODS

KEY RESOURCES TABLE

REAGENT or RESOURCE	SOURCE	IDENTIFIER
Antibodies		
KZ52	(Maruyama et al., 1999); this study	N/A
c2G4, c4G7, c13C6	(Audet et al., 2014); this study	N/A
mAb-100	(Misasi et al., 2016); this study	N/A
FVM04	(Howell et al., 2016); M.J. Aman	N/A
MR72	(Flyak et al., 2015); J.E. Crowe	N/A
h21D10	(Holtsberg et al., 2015); M.J. Aman	N/A
3C10	USAMRIID	N/A
Adimab human antibody collection from EBOV disease survivor	(Bornholdt et al., 2016b); Adimab, LLC	Sequences deposited in GenBank; see Table S3 for list of accession numbers
ADI-15878 inferred germline variants	This study	N/A
Bacteria and Viruses		
rVSV-EBOV/Mayinga GP (EBOV/H.sap-tc/COD/76/Yambuku-Mayinga)	(Wong et al., 2010); this study	N/A
rVSV-EBOV/Makona GP (EBOV/H.sap-rec/LBR/14/Makona-L2014)	(Bornholdt et al., 2016a); this study	N/A
rVSV-SUDV/Boneface GP (SUDV/C.por-lab/SSD/76/Boneface)	(Wec et al., 2016); this study	N/A
rVSV-BDBV GP (BDBV/H.sap/UGA/07/But-811250	(Wec et al., 2016); this study	N/A
Pseudotype VSV-TAFV GP (TAFV/H.sap-tc/CIV/94/CDC807212)	(Misasi et al., 2012); this study	N/A
Pseudotype VSV-MARV/Musoke GP (MARV/H.sap-tc/KEN/80/Mt. Elgon-Musoke)	(Misasi et al., 2012); this study	N/A
rVSV-RESTV GP (RESTV/M.fas-tc/USA/89/Phi89-AZ-1435	(Wec et al., 2016); this study	N/A
rVSV-LLOV GP (LLOV/M.sch-wt/ESP/03/Asturias-Bat86)	(Ng et al., 2014); this study	N/A
Mouse-adapted EBOV/Mayinga (EBOV-MA) (EBOV/M.mus-tc/COD/76/Yambuku-Mayinga)	(Bray et al., 1998); USAMRIID	N/A
EBOV/Kikwit (Ebola virus/H. sap-tc/COD/1995/Kikwit-9510621)	(Jahrling et al., 1999); USAMRIID	N/A
SUDV/Boneface (Sudan virus/H. sap-gp-tc/SDN/1976/Boneface-USAMRIID111808)	(Brannan et al., 2015); USAMRIID	N/A
BDBV (Bundibugyo virus/H. sap-tc/UGA/2007/Bundibugyo-200706291)	(Towner et al., 2008); USAMRIID	N/A
Chemicals, Peptides, and Recombinant Proteins		
Recombinant human Cathepsin L	R&D Systems	952-CY-010
Cysteine cathepsin inhibitor E-64	Peptides International	IES-4096; CAS: 66701-25-5
Thermolysin	Sigma-Aldrich	T7902; CAS: 9073-78-3
Phosphoramidon	Peptides International	IPO-4082; CAS: 119942-99-3
Freestyle 293 expression medium	Thermo Fisher	12338002
Soluble GP EBOVΔTM	(Bornholdt et al., 2016b); this study	N/A
Soluble NPC1 domain C-flag	(Miller et al., 2012); this study	N/A

(*Continued on next page*)

Continued

REAGENT or RESOURCE	SOURCE	IDENTIFIER
Ultra-TMB colorimetric substrate	Thermo Fisher	34029
Function-spacer-lipid construct (FSL-biotin)	Sigma-Aldrich	F9182
Streptavidin	Jackson Immuno Research	016-000-113
Deposited data		
ADI-15742 Fab complex with EBOV GPΔTM	This paper	EMDB: EMD-8699
ADI-15878 Fab complex with EBOV GPΔTM	This paper	EMDB: EMD-8700
ADI-15946 Fab complex with EBOV GPΔTM	This paper	EMDB: EMD-8701
ADI-16061 Fab complex with EBOV GPΔTM	This paper	EMDB: EMD-8698
Experimental Models: Cell Lines		
HEK293T	ATCC	CRL-3216
293-Freestyle	Thermo Fisher	R79007
Vero	ATCC	CCL-81
Vero C1008 cells (VERO 76, clone E6, Vero E6)	ATCC	CRL-1586
Experimental Models: Organisms/Strains		
Mouse: Female BALB/cAnNCrl	Charles River	Strain code: 028
Mouse: B6.129S2-Ifnar1tm1Agt/Mmjax (Type 1 IFNα/βR−/−)	Jackson Labs	MMRRC: 32045-JAX
Ferret: Outbred *Mustela putorius furo*	Marshall BioResources	N/A
Recombinant DNA		
pCAGGS-TAFV GP	(Misasi et al., 2012); this study	N/A
Sequence-based reagents		
BDBV GP sequencing primer Fwd01: AGCCCAATGCAGCTTTCAGA	IDT; this study	N/A
BDBV GP sequencing primer Fwd02: GACCTAGAGCGCTGCCTTC	IDT; this study	N/A
BDBV GP sequencing primer Fwd02: GACCTAGAGCGCTGCCTTC	IDT; this study	N/A
BDBV GP sequencing primer Rev02: CCCCAGCTTCGTAGTTCACC	IDT; this study	N/A
BDBV GP sequencing primer Fwd03: GATTCCGAGCTGGTGTTCCA	IDT; this study	N/A
BDBV GP sequencing primer Rev03: GGTTCATGTAGTGGTGGCGA	IDT; this study	N/A
BDBV GP sequencing primer Fwd04: ATCCCCCAGACAACACAACC	IDT; this study	N/A
BDBV GP sequencing primer Rev04: TAAACCAATGGCAGCCCCTT	IDT; this study	N/A
BDBV GP sequencing primer Fwd05: CAGCGAGTCTACAGAGCCAG	IDT; this study	N/A
BDBV GP sequencing primer Fwd06: GGCTAATTTGCGGGTTGAGG	IDT; this study	N/A
BDBV GP sequencing primer Rev06: AGAGGCCATTATGCTGGTACA	IDT; this study	N/A
Software and Algorithms		
Appion	(Lander et al., 2009)	http://emg.nysbc.org/redmine/projects/appion/wiki/Appion_Home
UCSF Chimera	(Pettersen et al., 2004)	https://www.cgl.ucsf.edu/chimera/
Pymol Molecular Graphics System	Schrödinger, LLC	http://www.pymol.org
CLUSTALW	(Larkin et al., 2007)	http://www.clustal.org
MATLAB	MathWorks	http://www.mathworks.com

(*Continued on next page*)

Continued

REAGENT or RESOURCE	SOURCE	IDENTIFIER
color_b.py	Robert L. Campbell	http://pldserver1.biochem.queensu.ca/~rlc/work/pymol/
EMAN2	(Tang et al., 2007)	http://blake.bcm.edu/emanwiki/EMAN2
DoGpicker	(Voss et al., 2009)	http://emg.nysbc.org/redmine/projects/software/wiki/DoGpicker
Other		
CellInsight CX5 High Content Screening (HCS) Platform	Thermo Fisher	CX51110
Zeiss Axio Observer.Z1 inverted fluorescence microscope	Carl Zeiss AG	N/A
Octet RED96 System	ForteBio, Pall LLC	http://www.fortebio.com/octet-RED96.html
Anti-human Fc (AHC) capture sensors	ForteBio, Pall LLC	18-5060

CONTACT FOR REAGENT AND RESOURCE SHARING

Further information and requests for resources and reagents should be directed to and will be fulfilled by the Lead Contact, Zachary A. Bornholdt (zachary.bornholdt@mappbio.com).

EXPERIMENTAL MODEL AND SUBJECT DETAILS

Cell lines

Vero female African grivet monkey cells, HEK293T female human embryonic kidney fibroblast cells, and U2OS female human osteosarcoma cells were obtained from the American Type Culture Collection (ATCC). Vero and HEK293T cells were cultured in high-glucose Dulbecco's modified Eagle medium (DMEM; Thermo Fisher) supplemented with 10% fetal bovine serum (Atlanta Biologicals), 1% GlutaMAX (Thermo Fisher), and 1% penicillin-streptomycin (Thermo Fisher). U2OS cells were cultured in McCoy's-5A medium (Thermo Fisher) with serum and additives as above. Suspension-adapted 293-Freestyle (293-F) cells were obtained from Thermo Fisher, and cultivated in Freestyle 293 serum-free expression medium (Thermo Fisher). Cell lines were maintained in a humidified 37°C incubator supplied with 5% CO2 (Vero, HEK293T) or 8% CO2 (293-F). Cell lines were not authenticated following purchase.

Vesicular stomatitis virus (VSV) recombinants and pseudotypes

Recombinant vesicular stomatitis Indiana viruses (rVSV) expressing eGFP in the first position, and encoding representative GP proteins from EBOV/Mayinga (EBOV/H.sap-tc/COD/76/Yambuku-Mayinga), EBOV/Makona (EBOV/H.sap-rec/LBR/14/Makona-L2014), BDBV (BDBV/H.sap/UGA/07/But-811250), SUDV/Boneface (SUDV/C.por-lab/SSD/76/Boneface), RESTV (RESTV/M.fas-tc/USA/89/Phi89-AZ-1435), and LLOV (LLOV/M.sch-wt/ESP/03/Asturias-Bat86), in place of VSV G have been described previously (Ng et al., 2014; Wec et al., 2016; Wong et al., 2010). VSV pseudotypes bearing eGFP and GP proteins from TAFV (TAFV/H.sap-tc/CIV/94/CDC807212) and MARV (MARV/H.sap-tc/KEN/80/Mt. Elgon-Musoke) were generated as described (Takada et al., 1997).

Authentic filoviruses

The authentic filoviruses EBOV/"Zaire 1995" (EBOV/H.sap-tc/COD/95/Kik-9510621) (Jahrling et al., 1999), mouse-adapted EBOV/Mayinga (EBOV-MA) (Bray et al., 1998), SUDV/Boneface-USAMRIID111808 (WHO International Study Team, 1978), and BDBV/200706291 (Towner et al., 2008) were used in this study.

METHOD DETAILS

Generation of cleaved VSV-GP particles and GPΔTM ectodomain proteins

In some experiments, cleaved viral particles bearing GP_{CL} were first generated by incubation with thermolysin (200 μg/mL, pH 7.5, 37°C for 1 h; Sigma-Aldrich) or recombinant human cathepsin L (CatL, 2 ng/μL, pH 5.5, 37°C for 1 h; R&D Systems), as described previously (Wong et al., 2010). Reactions were stopped by removal onto ice and addition of phosphoramidon (1 mM) or E-64 (10 μM), respectively, and viral particles were used immediately for infectivity assays. A recombinant, soluble GPΔTM protein (Bornholdt et al., 2016b) was also cleaved essentially as described above.

VSV infectivity measurements and neutralization assays

Viral infectivities were measured by automated counting of eGFP+ cells (infectious units; IU) using a CellInsight CX5 imager (Thermo Fisher) at 12–14 hr post-infection. For mAb neutralization experiments, pre-titrated amounts of VSV-GP particles (MOI ≈ 1 IU per cell)

were incubated with increasing concentrations of test mAb at room temp for 1 hr, and then added to confluent cell monolayers in 96-well plates. Viral neutralization data were subjected to nonlinear regression analysis to derive EC_{50} values (4-parameter, variable slope sigmoidal dose-response equation; GraphPad Prism).

Authentic filovirus microneutralization assays

Antibodies were diluted to indicated concentrations in culture media and incubated with virus for 1 hr. Vero E6 cells were exposed to antibody/virus inoculum at an MOI of 0.2 (EBOV, BDBV) or 0.5 (SUDV) plaque-forming unit (PFU)/cell for 1 hr. Antibody/virus inoculum was then removed and fresh culture media was added. At 48 hr post-infection, cells were fixed, and infected cells were immunostained using 3C10 antibody and quantitated by automated fluorescence microscopy, as described (Wec et al., 2016).

Generation of mAbs

Antibodies used for initial binding and neutralization screening, as well as germline-reverted (IGL) mAb constructs and WT:IGL chimeras of ADI-15878, were expressed in *Saccharomyces cerevisiae* as described previously (Bornholdt et al., 2016b). Briefly, yeast cultures were grown in 24-well plates, harvested by centrifugation after 6 days, and IgGs were purified by protein A-affinity chromatography. IgGs used in in vivo challenge experiments were expressed in FreeStyle™ 293-F cells by transient co-transfection of heavy and light chain plasmids (ThermoFisher). One day prior to transfection, HEK293 cells were passaged at 2.0–2.5 × 10^6 cells per ml. On the day of transfection, cells were pelleted by centrifuging at 400 ×g for 5 min, and cell pellets were resuspended in fresh FreeStyle F17 medium at a density of 4 × 10^6 cell per ml and returned to the incubator. A transfection mixture was prepared by first diluting the plasmid DNA preparations in FreeStyle F17 medium (1.33 μg total plasmid DNA per ml of culture). Transfection agent, PEIpro (Polyplus Transfection, Illkirch, France), was then added to the diluted DNA at a DNA-to-PEI ratio of 1:2, and the mixture was incubated at room temperature for 10 min. The transfection mixture was then added to the culture. Cultures were harvested six days post transfection by two rounds of centrifugation, each at 2000 ×g for 5 min, and antibodies were purified the clarified conditioned medium by passing over Protein A agarose (MabSelect SuRe from GE Healthcare Life Sciences). The bound antibodies were washed with PBS, eluted with 200 mM acetic acid[pH 3.5],50 mM NaCl into 1/8th volume 2M HEPES[pH 8.0], and buffer-exchanged into PBS.

Fabs were generated by digesting the IgGs with papain for 2 hr at 30°C. Reactions were terminated by the addition of iodoacetamide, and the Fab and Fc mixtures were passed over Protein A agarose to remove Fc fragments and undigested IgG. The flow-through was then passed over CaptureSelect IgG-CH1 affinity resin (ThermoFisher), and eluted and buffer-exchanged as above.

ELISAs for GP:mAb binding

To identify GP cross-reactive mAbs in Figures 1 and S1, normalized amounts of rVSVs bearing EBOV, BDBV, and SUDV GP were coated onto plates at 4°C. Plates were then blocked with PBS containing 3% bovine serum albumin (PBSA), and incubated with dilutions of test antibody (5, 50 nM). Bound Abs were detected with anti-human IgG conjugated to horseradish peroxidase (Santa Cruz Biotechnology) and Ultra-TMB colorimetric substrate (Thermo Fisher). All incubations were performed for 1 hr at 37°C.

Competition ELISAs for GP/mAb binding to NPC1

The viral lipid envelopes of rVSV-EBOV GP particles were labeled with biotin using a function-spacer-lipid construct (FSL-biotin) (Sigma-Aldrich) for 1 hr at pH 7.5 and 37°C, as described (Ng et al., 2014). Biotinylated viral particles bearing GP_{CL} were generated by incubation with thermolysin, and then captured onto high-binding 96-well ELISA plates precoated with recombinant streptavidin (0.65 μg/mL; Sigma-Aldrich). Plates were then blocked with PBSA, and incubated with serial dilutions of test mAbs. Washed plates were then incubated with a pre-titrated concentration of soluble, FLAG epitope-tagged, NPC1 domain C (NPC1–C) protein (Bornholdt et al., 2016a), and bound NPC1–C was detected with an anti-FLAG antibody conjugated to horseradish peroxidase (Sigma-Aldrich). All incubations were performed for 1 hr at 37°C.

ELISAs and immunoblots to detect mAb inhibition of GP cleavage

In Figure 5B, we used exposure of the NPC1-binding site in EBOV GP_{CL} as a proxy for successful GP → GP_{CL} cleavage by CatL. rVSV-EBOV GP particles, biotinylated as above, were preincubated with mixtures of test mAb and irrelevant human IgG (test mAb at 50, 250, or 1000 nM; 1000 nM total IgG per reaction) for 1 hr at pH 5.5 and 37°C. Reactions were then incubated with CatL (4 ng/μL and 37°C for 30 min). Reactions were then stopped with the cysteine cathepsin inhibitor E-64, readjusted to neutral pH with PBS, and captured onto streptavidin-coated ELISA plates. NPC1–C binding was measured as above.

Samples treated with the highest concentration of test mAb were also subjected to western blotting (Figure 5C). Cleaved GP1 species were detected by immunoblotting with h21D10 mAb (a gift from Dr. Javad Aman) directly conjugated to horseradish peroxidase.

Selection of viral neutralization escape mutants

Escape mutant selections were performed by serial passage of rVSV-GP particles in the presence of test mAb. Briefly, serial 3-fold dilutions of virus were preincubated with a concentration of mAb corresponding to the IC_{90} value derived from neutralization assays, and then added to confluent monolayers of Vero cells in 12-well plates, in duplicate. Infection was allowed to proceed to completion (> 90% cell death by eye), and supernatants were harvested from the infected wells that received the highest dilution (i.e., the least

amount) of viral inoculum. Following three subsequent passages under mAb selection with virus-containing supernatants as above, supernatants from passage 4 were tested for viral neutralization escape. If resistance was evident, individual viral clones were plaque-purified on Vero cells, and their *GP* gene sequences were determined as described previously (Wong et al., 2010). The following escape mutant selections were performed: ADI-16061 with rVSV-EBOV/Makona GP, ADI-15742 with rVSV-SUDV/Boneface GP, ADI-15750 with rVSV-EBOV/Mayinga GP, and ADI-15946 with mucin domain-deleted rVSV-BDBV GPΔMuc.

Single-particle electron microscopy

Antibody Fabs and a EBOV GPΔTM ectodomain protein were prepared as above, and incubated at a ratio of 10:1 (Fab:GP) overnight at 4°C. Complexes were then deposited onto a carbon-coated copper mesh grid, and stained with 1% uranyl formate. Samples were imaged on a Tecnai F12 microscope using the automated image acquisition software Leginon (Suloway et al., 2005). Images were collected with a Tietz 4K CMOS detector at 52,000 × magnification, resulting in a final pixel size of 2.05Å at the specimen level. Images were automatically uploaded to and processed within our Appion database (Lander et al., 2009). Individual complexes were extracted from raw images using DoG Picker (Voss et al., 2009), binned by 2, and placed into a stack. The stack was then subjected to reference-free 2D classification using MRA/MSA (Ogura et al., 2003). Class averages that did not respond to Fab:EBOV GPΔTM complexes were removed from all subsequent analyses. A subset of 2D class averages was used to create an initial model using common lines within EMAN2 (Tang et al., 2007). The raw particle stack was then refined against the initial model using EMAN2 to yield the final 3D volumes. UCSF Chimera was used for modeling and figure generation (Goddard et al., 2007).

Structural representation of ebolavirus GP sequence conservation

To graphically represent the degree of sequence conservation of each surface-exposed residue in the ebolavirus GP trimer (Figure 4), representative GP sequences from EBOV, TAFV, BDBV, SUDV, and RESTV were aligned with CLUSTALW (Larkin et al., 2007). This multiple sequence alignment was submitted to the AL2CO server (Pei and Grishin, 2001) to calculate a normalized conservation score at each amino acid position, using a BLOSUM62 matrix. To color residues in the EBOV GPΔTM X-ray crystal structure [PDB: 5JQ3; (Zhao et al., 2016)] according to sequence conservation, the crystallographic B-factor associated with each residue in the PDB file was first replaced with the conservation score using a custom MATLAB script. Residues in this modified PDB file were then recolored in MacPymol (Schrödinger) using the script color_b.py (Robert Campbell, http://pldserver1.biochem.queensu.ca/~rlc/work/pymol/). A 3-color histogram was used to evenly assign ranges of conservation scores to ranges of colors.

GP:mAb kinetic binding analysis by biolayer interferometry (BLI)

The Octet Red^{TM} system (FortéBio, Pall) was used to determine the binding properties of different IgGs to various forms of EBOV GP. Anti-human Fc (AHC) capture sensors (ForteBio) were used for initial mAb loading at 25 mg/mL in 1 × kinetics buffer (PBS supplemented with 0.002% Tween-20 and 1 mg/mL of BSA). Binding to GP was performed across two-fold serial dilutions of EBOV GPΔTM or GP_{CL}. The baseline and dissociation steps were carried out in the 1 × kinetics buffer as per the instrument manufacturer's recommendations. For analysis of binding at pH 5.5, a 1 × pH 5.5 kinetics buffer (50 mM sodium citrate dihydrate[pH 5.5], 150 mM sodium chloride, 0.002% Tween-20 and 1 mg/mL BSA) was used in place of the PBS-based 1 × kinetic buffer for all steps. Kinetic binding data in all cases are adequately described accurately by a 1:1 binding model (Figures S6A and S6B), but given the bivalent nature of the IgG (immobilized) and the trimeric state of GP (analyte), the association stoichiometry is likely to be more complex. Thus, k_{off}/k_{on} likely reflects an ensemble of binding stoichiometries, and accordingly, we refer to this ratio as apparent K_D (K_d^{app}) throughout.

EBOV and SUDV challenge studies in mice

10–12 week old female BALB/c mice (Jackson Labs) were challenged via the intraperitoneal (i.p.) route with EBOV-MA (100 PFU; ~3,000 LD_{50}). Mice were treated i.p. 2 days post-challenge with PBS vehicle or 300 μg of each mAb (0.3 mL volume, ≈15 mg mAb/kg). Animals were observed daily for clinical signs of disease and lethality. Daily observations were increased to a minimum of twice daily while mice were exhibiting signs of disease. Moribund mice were humanely euthanized on the basis of IACUC-approved criteria.

6–8 week old male and female Type 1 IFN α/β receptor knockout mice (Type 1 IFNα/β R−/−) (Jackson Labs) were challenged with WT SUDV (1000 PFU i.p.). Animals were treated i.p. 1 and 4 days post-challenge with PBS vehicle or 300 μg (≈15 mg mAb/kg) per dose, and monitored and euthanized as above.

BDBV challenge studies in ferrets

Six-month-old ferrets (*Mustela putorius furo*) were challenged via the intramuscular (i.m.) route with WT BDBV (BDBV/H.sap-tc/UGA/07/Butalya-811250; 1000 $TCID_{50}$ in 0.5 mL volume), as described previously (Kozak et al., 2016). Animals were treated i.p. 3 and 6 days post-challenge with either PBS vehicle or 15 mg (day 3) and 10 mg (day 6) of each mAb (2 mL volume/dose). Additionally, 1 mL blood was taken from each animal on days 0, 3, 6, 10, 14, 21, 28 days post-infection to determine viral load, measure complete blood counts, and evaluate biochemical markers. Animals were monitored twice daily for signs of disease during the course of the experiment.

BDBV GP sequencing from ferret blood samples

Total RNA was extracted from ferret blood samples at 3, 6, 10, and 14 days post-challenge with the QIAamp Viral RNA Mini Kit (QIAGEN). RNA was reverse transcribed with SuperScript IV VILO Master Mix (Thermo Fisher) according to the manufacturer's instructions. PCR reaction conditions were as follows: 45 cycles of 95°C for 30 s, 55°C for 30 s, and 72°C for 60 s. PCR product purification from the agarose gel was performed with the NucleoSpin gel and PCR clean-up kit (Macherey-Nagel), and subjected to Sanger DNA sequencing. The sequences were aligned to that of the challenge virus preparation and the published BDBV GP sequence (Bundibugyo virus/H. sap-tc/UGA/2007/Bundibugyo-200706291; GenBank accession number KU182911.1). Sequencing primers are indicated in the Key Resources Table.

Animal welfare statement

Murine challenge studies were conducted under IACUC-approved protocols in compliance with the Animal Welfare Act, PHS Policy, and other applicable federal statutes and regulations relating to animals and experiments involving animals. The facility where these studies were conducted (USAMRIID) is accredited by the Association for Assessment and Accreditation of Laboratory Animal Care, International (AAALAC) and adhere to principles stated in the Guide for the Care and Use of Laboratory Animals, National Research Council (2011). The animal facility at USAMRIID performs routine clinical observations to evaluate anorexia, activity, dehydration and edema. Mice were observed daily by assigned Veterinary Medicine Division personnel for husbandry conditions, humane care and general health. All procedures for animal care and housing are in accordance with the NRC Guide for the Care and Use of Laboratory Animals (1996) (Clark et al., 1997) and the Animal Welfare Act as amended and standards incorporated in 9 CFR Part 3, 1991. For all mouse studies described, mice were purchased from commercial suppliers and housed in microisolator cages (10 mice per cage) with water and food provided ad libitum. Once received, mice were placed in quarantine and evaluated for the presence of parasites, infectious agents, or other conditions that could adversely affect the studies. At the end of the quarantine period an American College of Laboratory Animal Medicine (ACLAM)-certified veterinarian released the animals for use in studies once they were determined to be healthy. All mice used for the described studies were naive animals that had not previously been used for any other study or previously exposed to test antibodies or viruses.

Ferret challenge studies were approved by the Animal Care Committee (ACC) of the Canadian Science Centre for Human and Animal Health (CSCHAH) in Winnipeg, Canada, in accordance with guidelines from the Canadian Council on Animal Care (CCAC). Ferrets were obtained from Marshall BioResources USA, and were monitored daily for food and water consumption and given environmental enrichment according to the guidelines for the species. Cage cleaning and complete bedding exchange was carried out three times per week. Two or three animals were housed per cage in the Allentown caging system. Each unit is ventilated with a HEPA blower system and all units are manufactured from stainless steel and are autoclavable. Following viral challenge, survival, weight, temperature and overall health were monitored daily and recorded on the humane scoring chart. Ferretsused for BDBV challenges were previously involved in a non-interventional influenza A virus (IAV subtype H5N1) pathogenesis study. Thy were challenged with IAV, and did seroconvert by ELISA, but did not present with disease symptoms. No treatments or vaccinations were administered in that prior study. BDBV challenge was performed 40 days after the IAV infection, a period sufficient for immune recovery of the animals.

QUANTIFICATION AND STATISTICAL ANALYSIS

Statistical details of experiments, including numbers of replicates (n), measures of precision (standard deviation, SD), and the statistical test(s) used can be found in the figure legends, figures, and Results. Dose-response neutralization curves were fit to a logistic equation by nonlinear regression analysis. 95% confidence intervals (95% CI) for the extracted IC_{50} parameter were estimated under the assumption of normality. Analysis of survival curves in Figure 7 was performed with the Mantel-Cox (log-rank) test. Statistical comparisons of viral titers in Figure 7F (also see Results) were carried out with a Mann-Whitney U test. Testing level (alpha) was 0.05 for all statistical tests. All analyses were carried out in GraphPad Prism.

DATA AND SOFTWARE AVAILABILITY

Sequences for all 349 mAbs from the Adimab collection (Bornholdt et al., 2016b) have been deposited in GenBank (see Table S3 for accession numbers). The accession numbers for the negative stain-EM reconstructions reported in this paper are Electron Microscopy Data Bank under accession numbers EMDB: EMD-8698–EMD-8701 (see Key Resources Table for details).

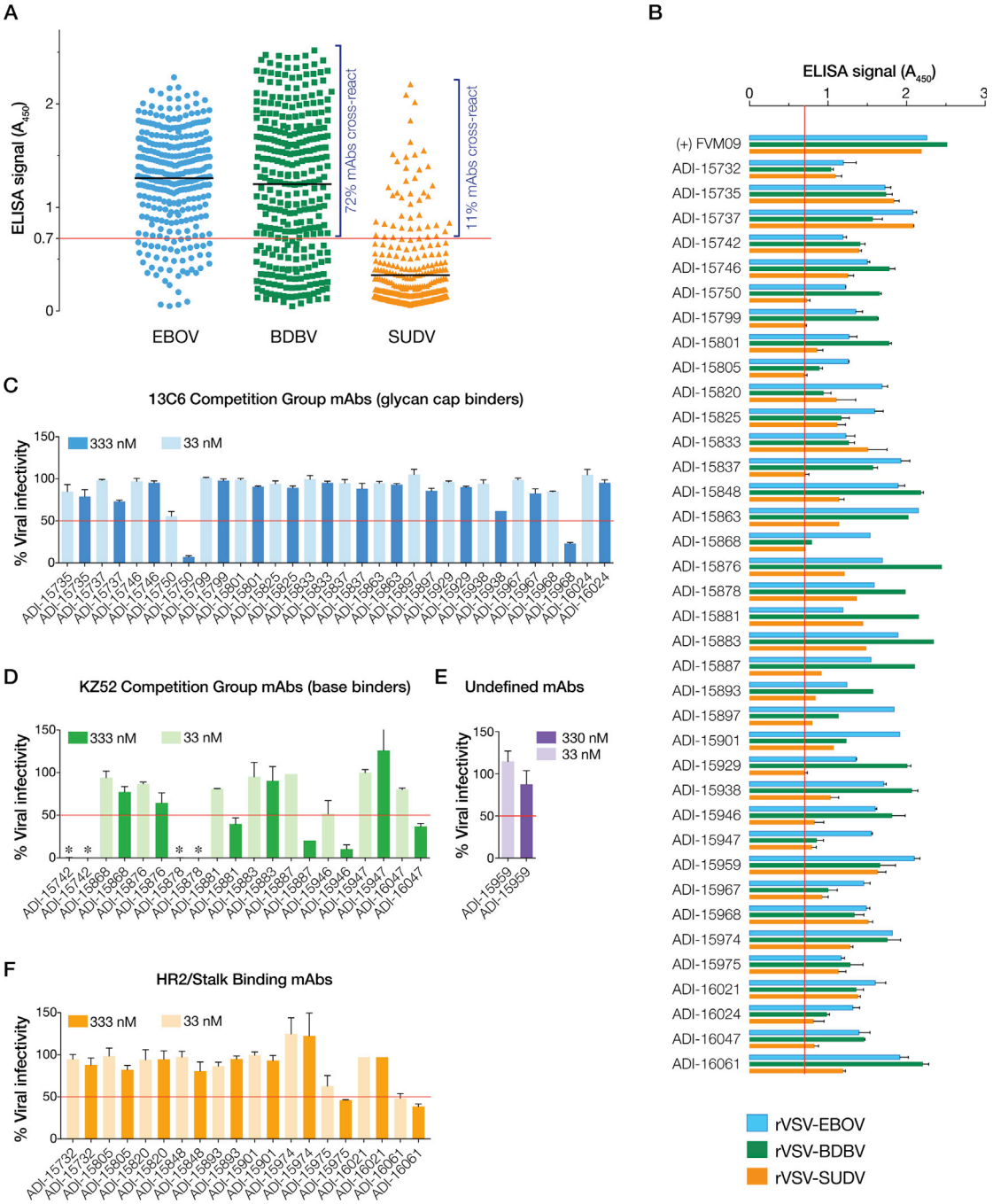

Figure S1. Screening a Collection of 349 Human EBOV Survivor mAbs for Pan-Ebolavirus Binders and Neutralizers, Related to Figure 1

(A) Capacity of mAbs to recognize rVSVs bearing EBOV, BDBV, and SUDV GP in an ELISA. A_{450}, absorbance at 450 nm. Red line indicates ELISA reactivity threshold for selecting cross-reactive mAbs, equivalent to 33% of the positive control.

(B) mAbs cross-reactive with SUDV GP in (A) were assayed for binding to rVSVs bearing EBOV, BDBV, and SUDV GP by ELISA. Means ± SD for three replicates are shown. Red line indicates ELISA reactivity threshold for selecting cross-reactive mAbs.

(C–F) Capacity of cross-reactive mAbs to neutralize rVSV-SUDV GP infection at two mAb concentrations. Means ± standard deviation (SD) for three replicates are shown. Asterisks, infectivity below the detection limit. Red line indicates neutralization efficacy threshold for selecting cross-neutralizing mAbs. mAbs are binned by competition/epitope group.

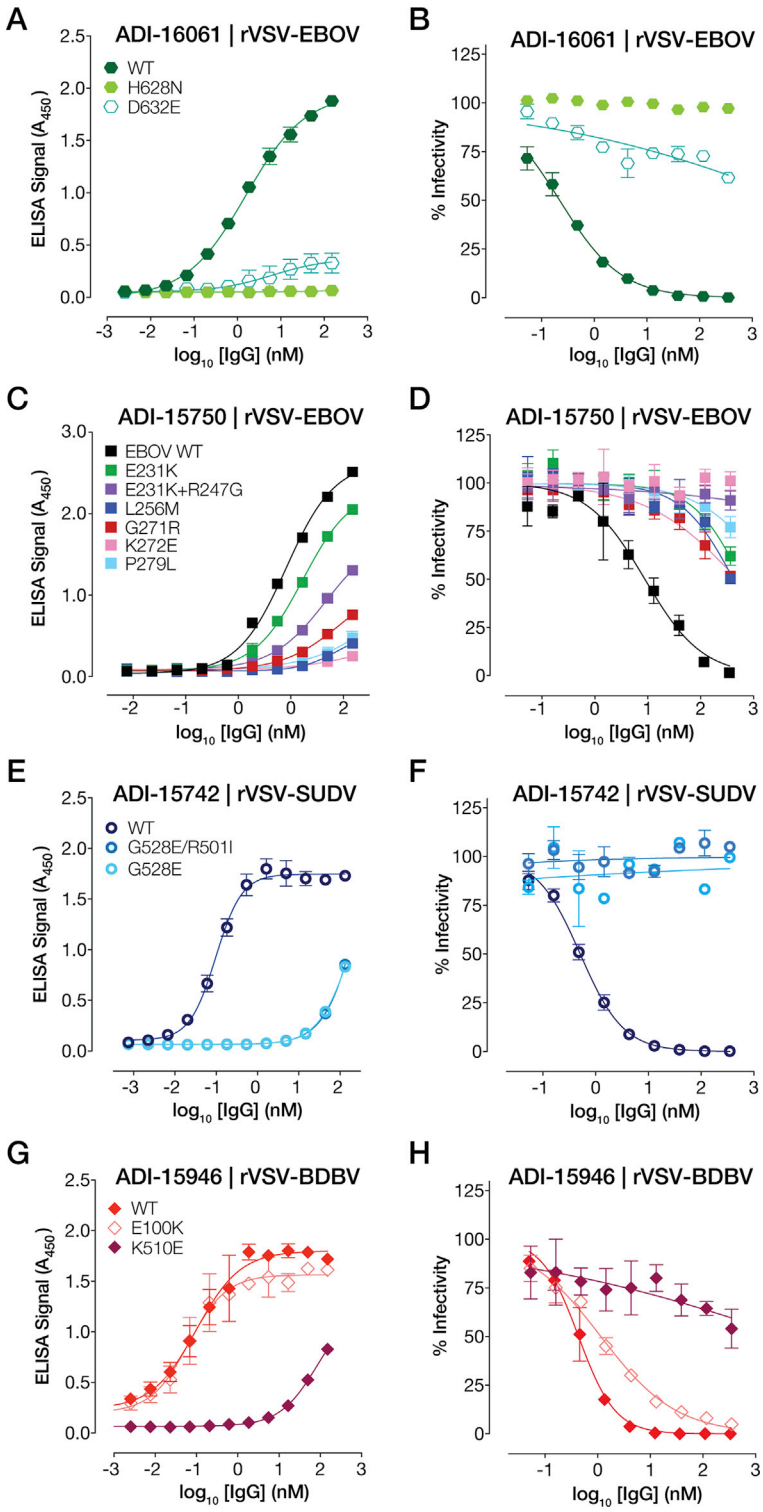

Figure S2. Characterization of Viral Mutants Resistant to mAb Neutralization, Related to Figure 3

rVSV-GP mutants resistant to each broadly neutralizing mAb were selected and isolated as described in STAR Methods.

(A, C, E, and G) Capacity of NAbs to recognize rVSVs bearing GP neutralization-escape variants in an ELISA. Means ± SD for three replicates are shown.

(B, D, F, and H) Capacity of NAbs to neutralize rVSVs bearing GP neutralization-escape variants. Means ± SD for three replicates are shown.

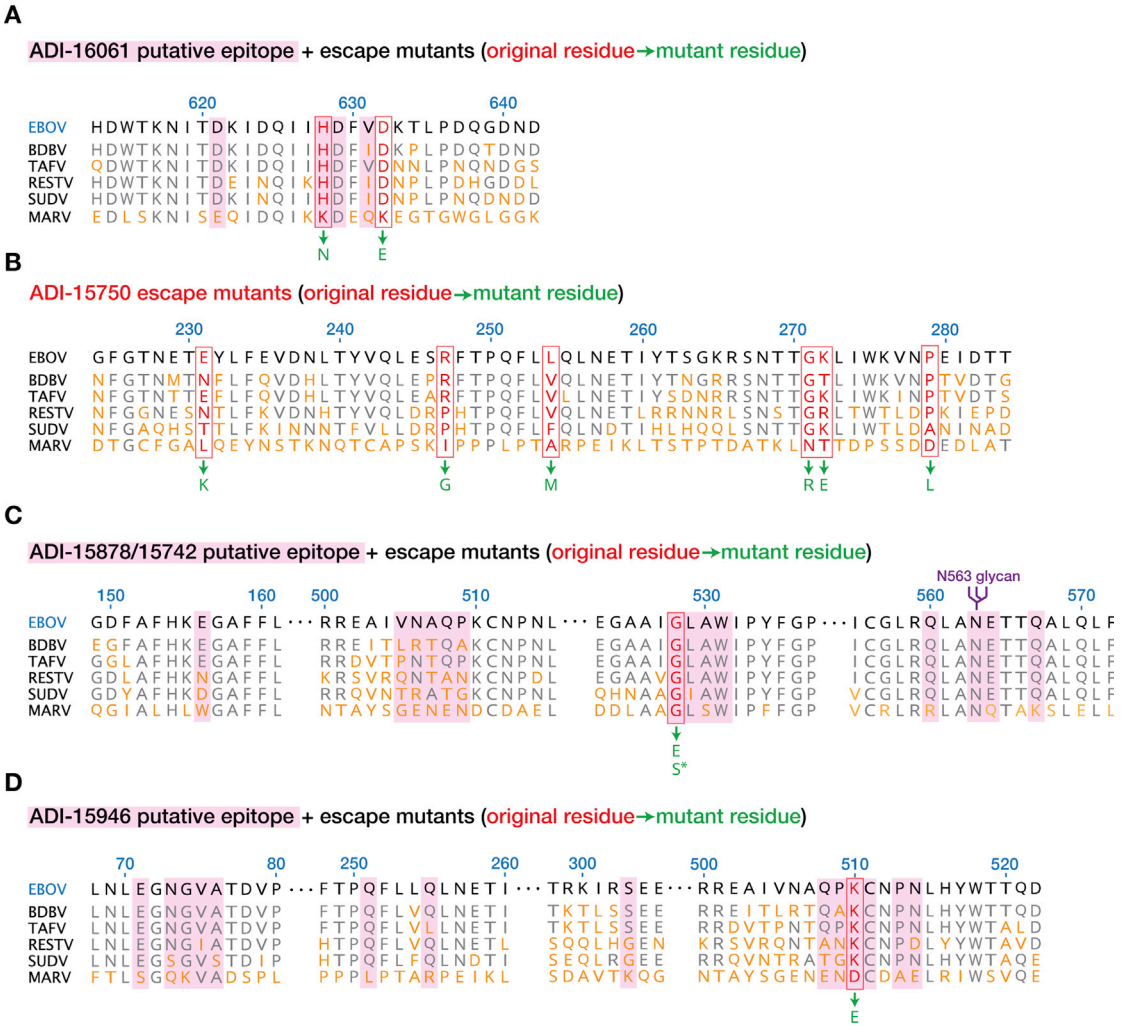

Figure S3. Locations of Viral Neutralization Escape Mutations and Putative NAb Epitopes in Filovirus GP, Related to Figure 3

(A–D) Amino acid sequence alignments of regions of filovirus GP encompassing each escape mutation and putative NAb epitope are shown (EBOV GP numbering). Gray, conserved residues. Orange, divergent residues. Putative NAb contact residues derived from the EM image reconstructions (Figure 3) are shaded in pink. Positions of escape mutations are boxed and labeled in red, and the residue changes are indicated in green. In (C), the location of the conserved N–linked glycan at residue 563 is indicated in purple.

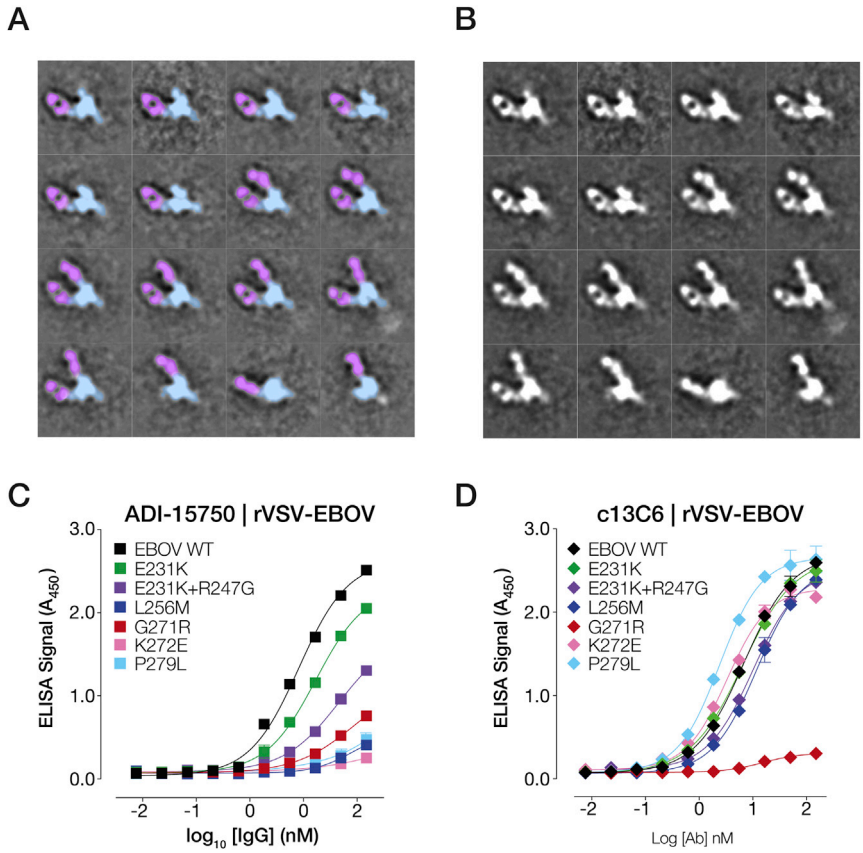

Figure S4. Sequence and Structural Properties of GP Recognition by ADI-15750, Related to Figure 3

(A and B) 2D class averages of the ADI-15750 FAb:EBOV GPΔTM complex derived by negative-stain EM are shown.

(A) Class averages are pseudocolored to highlight GP (cyan) and Fab (lilac).

(C and D) Capacity of ADI-15750 (C) and the glycan cap binder c13C6 (D) to recognize rVSV-EBOV GPs bearing ADI-15750—neutralization-escape variants in an ELISA. Means ± SD for three replicates are shown.

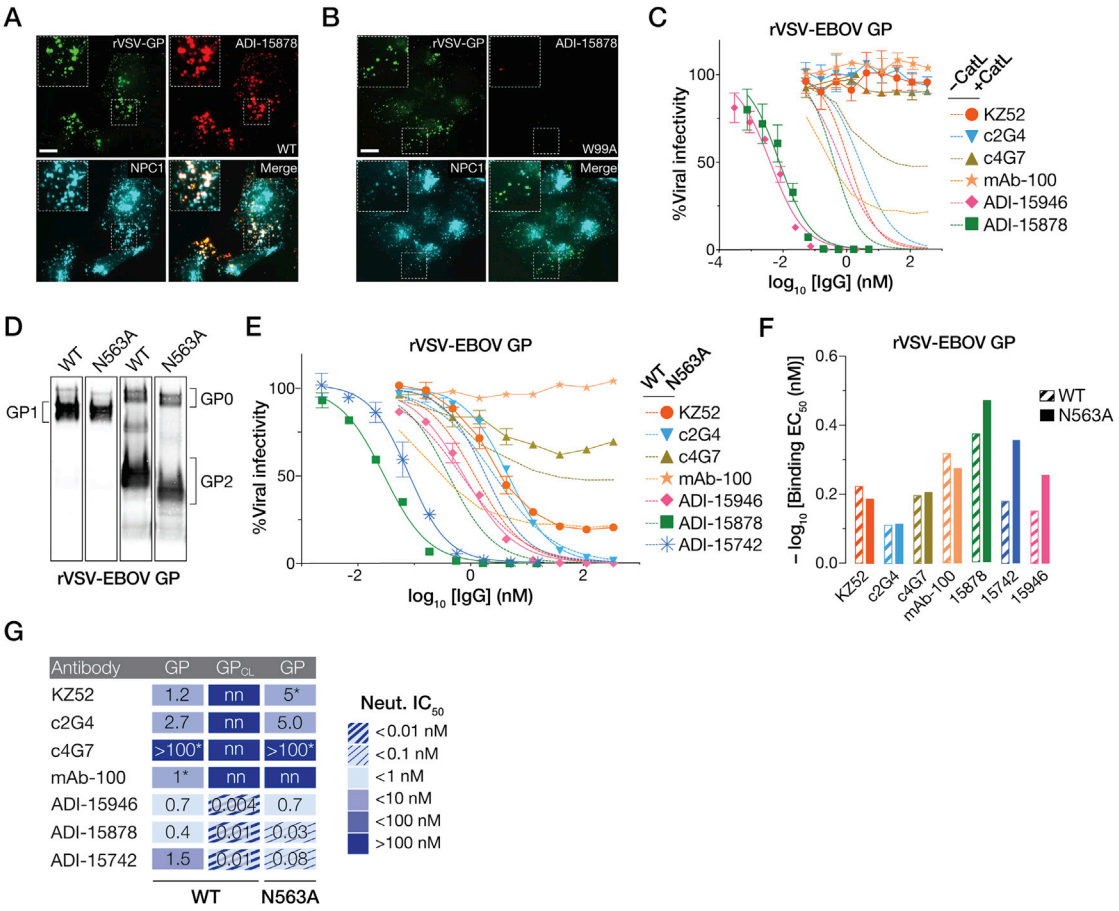

Figure S5. Delivery of ADI-15878 and Viral Particles to NPC1-Positive Endosomes and Effect of GP Cleavage and Glycosylation on mAb Neutralization Activity, Related to Figure 5

(A and B) Co-internalization of VSV-EBOV GP particles with ADI-15878^{WT} (A) and ADI-15878^{W99A} (B), and delivery to NPC1-positive endosomes. Scale bar, 20 μm.

(C) NAb neutralization dose curves of VSV particles bearing uncleaved (dotted lines) and CatL-cleaved EBOV GP proteins (solid lines and symbols). Means ± SD for three replicates are shown.

(D) GP2 bearing the N563A mutation displays increased electrophoretic mobility, consistent with removal of the glycan on residue N563. rVSV-GP particles bearing WT or N563A GP were resolved by SDS-PAGE and GP1 and GP2 were visualized by western blotting. GP0 is the uncleaved precursor of GP1 and GP2.

(E) NAb neutralization dose curves of VSV particles bearing EBOV GP (WT or N563A). WT, dotted lines. N563A, solid lines and symbols. Means ± SD for three replicates are shown.

(F) Capacity of NAbs to recognize EBOV GP (WT or N563A) in an ELISA. Log-transformed half-maximal binding concentrations (EC_{50}) derived from two independent binding dose curves are shown.

(G) Heatmaps and IC_{50} values for mAb neutralization of rVSVs bearing uncleaved and cleaved EBOV GP(WT) and uncleaved EBOV GP(N563A).

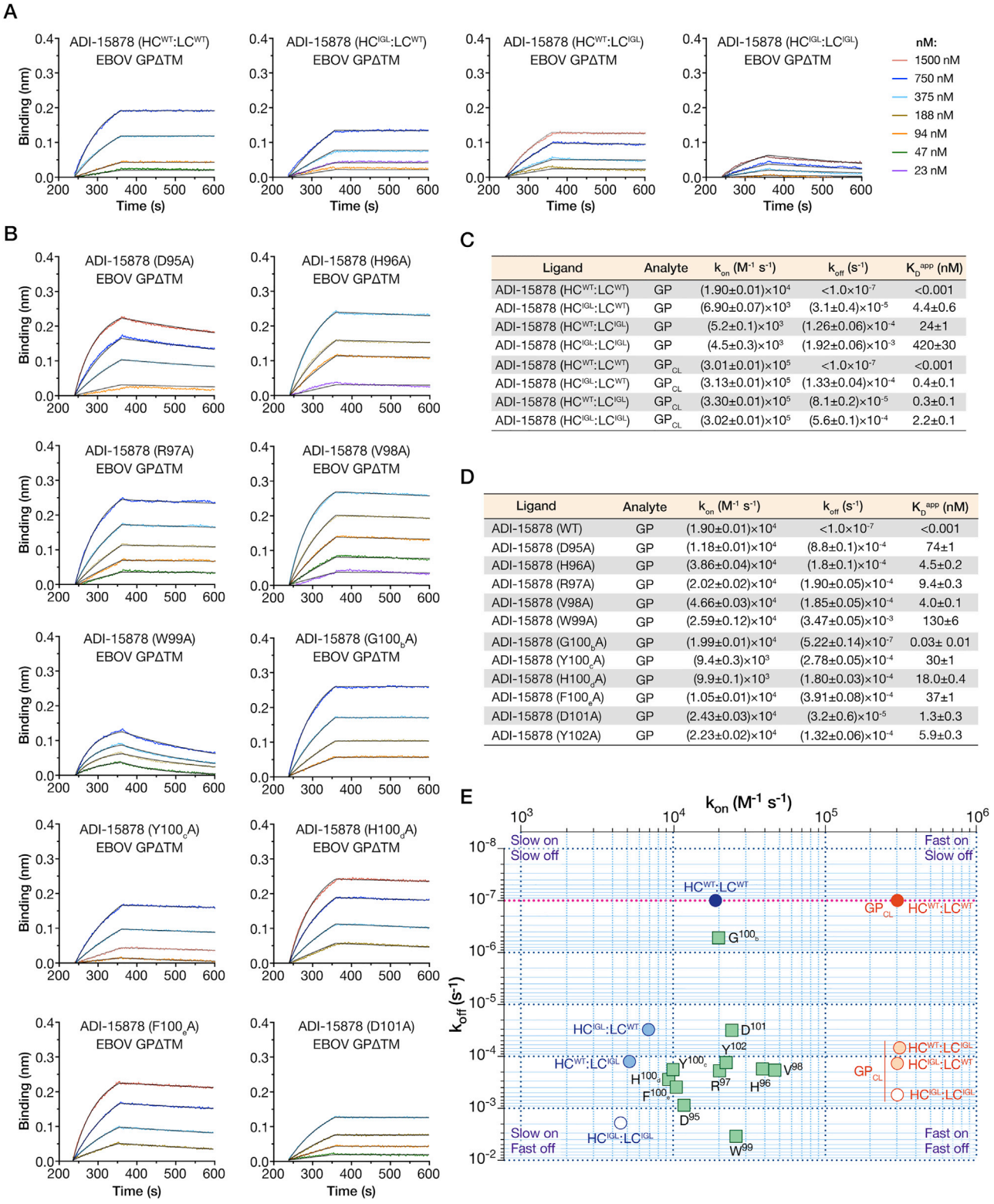

C

Ligand	Analyte	k_{on} (M^{-1} s^{-1})	k_{off} (s^{-1})	K_D^{app} (nM)
ADI-15878 (HC^{WT}:LC^{WT})	GP	$(1.90\pm0.01)\times10^4$	$<1.0\times10^{-7}$	<0.001
ADI-15878 (HC^{IGL}:LC^{WT})	GP	$(6.90\pm0.07)\times10^3$	$(3.1\pm0.4)\times10^{-5}$	4.4±0.6
ADI-15878 (HC^{WT}:LC^{IGL})	GP	$(5.2\pm0.1)\times10^3$	$(1.26\pm0.06)\times10^{-4}$	24±1
ADI-15878 (HC^{IGL}:LC^{IGL})	GP	$(4.5\pm0.3)\times10^3$	$(1.92\pm0.06)\times10^{-3}$	420±30
ADI-15878 (HC^{WT}:LC^{WT})	GP_{CL}	$(3.01\pm0.01)\times10^5$	$<1.0\times10^{-7}$	<0.001
ADI-15878 (HC^{IGL}:LC^{WT})	GP_{CL}	$(3.13\pm0.01)\times10^5$	$(1.33\pm0.04)\times10^{-4}$	0.4±0.1
ADI-15878 (HC^{WT}:LC^{IGL})	GP_{CL}	$(3.30\pm0.01)\times10^5$	$(8.1\pm0.2)\times10^{-5}$	0.3±0.1
ADI-15878 (HC^{IGL}:LC^{IGL})	GP_{CL}	$(3.02\pm0.01)\times10^5$	$(5.6\pm0.1)\times10^{-4}$	2.2±0.1

D

Ligand	Analyte	k_{on} (M^{-1} s^{-1})	k_{off} (s^{-1})	K_D^{app} (nM)
ADI-15878 (WT)	GP	$(1.90\pm0.01)\times10^4$	$<1.0\times10^{-7}$	<0.001
ADI-15878 (D95A)	GP	$(1.18\pm0.01)\times10^4$	$(8.8\pm0.1)\times10^{-4}$	74±1
ADI-15878 (H96A)	GP	$(3.86\pm0.04)\times10^4$	$(1.8\pm0.1)\times10^{-4}$	4.5±0.2
ADI-15878 (R97A)	GP	$(2.02\pm0.02)\times10^4$	$(1.90\pm0.05)\times10^{-4}$	9.4±0.3
ADI-15878 (V98A)	GP	$(4.66\pm0.03)\times10^4$	$(1.85\pm0.05)\times10^{-4}$	4.0±0.1
ADI-15878 (W99A)	GP	$(2.59\pm0.12)\times10^4$	$(3.47\pm0.05)\times10^{-3}$	130±6
ADI-15878 ($G100_bA$)	GP	$(1.99\pm0.01)\times10^4$	$(5.22\pm0.14)\times10^{-7}$	0.03± 0.01
ADI-15878 ($Y100_cA$)	GP	$(9.4\pm0.3)\times10^3$	$(2.78\pm0.05)\times10^{-4}$	30±1
ADI-15878 ($H100_dA$)	GP	$(9.9\pm0.1)\times10^3$	$(1.80\pm0.03)\times10^{-4}$	18.0±0.4
ADI-15878 ($F100_eA$)	GP	$(1.05\pm0.01)\times10^4$	$(3.91\pm0.08)\times10^{-4}$	37±1
ADI-15878 (D101A)	GP	$(2.43\pm0.03)\times10^4$	$(3.2\pm0.6)\times10^{-5}$	1.3±0.3
ADI-15878 (Y102A)	GP	$(2.23\pm0.02)\times10^4$	$(1.32\pm0.06)\times10^{-4}$	5.9±0.3

Figure S6. Summary of GP Binding Properties of ADI-15878 Variants, Related to Figure 6

(A and B) Kinetic binding curves for interaction between EBOV GPΔTM and ADI-15878 IGL variants (A) or CDR-H3 mutants (B) were determined by BLI. Each mAb was loaded onto probes, which were then dipped in solutions of the GPΔTM analyte at the indicated concentrations. Gray lines show curve fits to a 1:1 binding model.

(legend continued on next page)

(C) Kinetic binding constants for recognition of uncleaved and cleaved EBOV GPΔTM (GP and GP_{CL}, respectively) by WT and inferred germline (IGL) ADI-15878 variants were determined by BLI. HC, mAb heavy chain; LC, mAb light chain. k_{on}, association rate constant; k_{off}, dissociation rate constant; K_D^{app}, apparent equilibrium dissociation constant. 95% confidence intervals are reported for each binding constant.

(D) Kinetic binding constants for recognition of EBOV GPΔTM by ADI-15878 bearing the indicated mutations in the CDR-H3 loop were determined by BLI. 95% confidence intervals are reported for each binding constant.

(E) Graphical representation of the association and dissociation rate constants from (A) and (B). The lower limit of detection for the dissociation rate constant is shown as a pink line.

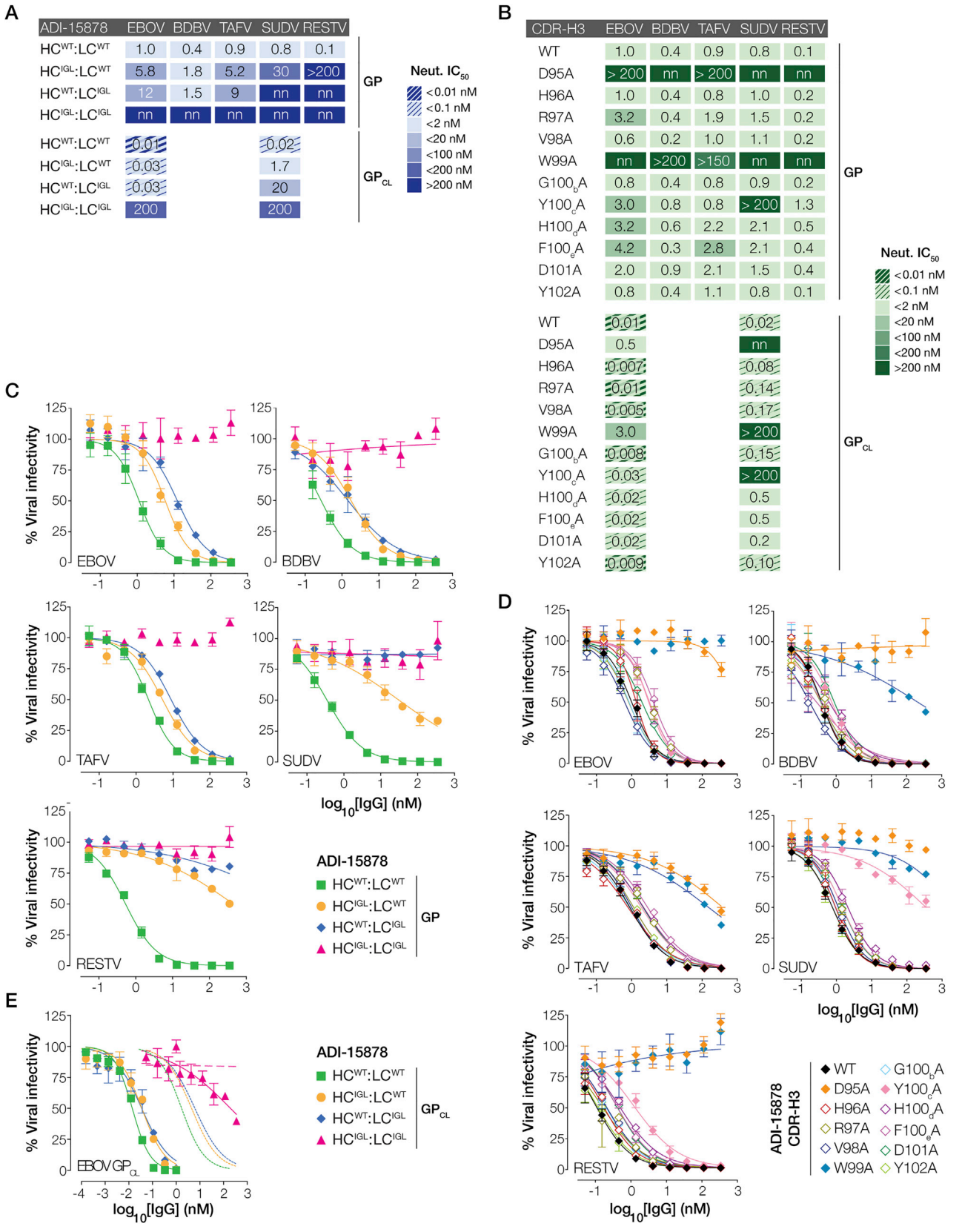

(legend on next page)

Figure S7. Summary of Viral Neutralization Properties of ADI-15878 Variants, Related to Figure 6

(A) Heatmaps and IC_{50} values for neutralization of rVSVs bearing uncleaved and cleaved ebolavirus GPs by ADI-15878 inferred-germline (IGL) variants. nn, non-neutralizing.

(B) Heatmaps and IC_{50} values for neutralization of rVSVs bearing uncleaved and cleaved ebolavirus GPs by ADI-15878 bearing the indicated mutations in the CDR-H3 loop.

(C and D) Neutralization dose curves from which data in (A) and (B) were derived.

(E) Dose curves for neutralization of cleaved rVSV-EBOV GP_{CL} particles by ADI-15878 IGL variants. Corresponding dose curves for uncleaved rVSV-EBOV GP are showed as dashed lines. In (C)–(E), means ± SD for three replicates are shown.